2016

Response of rigid piles during passive dragging

Wei Dong Guo
University of Wollongong, wdguo@uow.edu.au

Publication Details

Guo, W. (2016). Response of rigid piles during passive dragging. International Journal for Numerical and Analytical Methods in Geomechanics, 40 (14), 1936-1967.

Response of rigid piles during passive dragging

Abstract
This paper develops a three-layer model and elastic solutions to capture nonlinear response of rigid, passive piles in sliding soil. Elastic solutions are obtained for an equivalent force per unit length p_s of the soil movement. They are repeated for a series of linearly increasing p_s (with depth) to yield the nonlinear response. The parameters underpinning the model are determined against pertinent numerical solutions and model tests on passive free-head and capped piles. The solutions are presented in non-dimensional charts and elaborated through three examples. The study reveals the following:

- On-pile pressure in rotationally restrained, sliding layer reduces by a factor α, which resembles the p-multiplier for a laterally loaded, capped pile, but for its increase with vertical loading (embankment surcharge), and stiffness of underlying stiff layer: α=0.25 and 0.6 for a shallow, translating and rotating piles, respectively; α=0.33-0.5 and 0.8-1.3 for a slide overlying a stiff layer concerning a uniform and a linearly increasing pressure, respectively; and α=0.5-0.72 for moving clay under embankment loading.
- Ultimate state is well defined using the ratio of passive earth pressure coefficient over that of active earth pressure. The subgrade modulus for a large soil movement may be scaled from model tests.
- The normalised rotational stiffness is equal to 0.1-0.15 for the capped piles, which increases the pile displacement with depth.

The three-layer model solutions well predict nonlinear response of capped piles subjected to passive loading, which may be used for pertinent design.

Keywords
piles, during, passive, dragging, rigid, response

Disciplines
Engineering | Science and Technology Studies

Publication Details
Guo, W. (2016). Response of rigid piles during passive dragging. International Journal for Numerical and Analytical Methods in Geomechanics, 40 (14), 1936-1967.

Date revised: Nov/2013, Aug-Oct/014, Feb, April, June-August-September 2015

Title: Response of rigid piles during passive dragging

Wei Dong Guo

Affiliation and address:

Associate Professor Wei Dong Guo

School of Civil, Mining & Environmental Engineering

University of Wollongong, NSW 2522, Australia

Email: camsaweidguo@lycos.com; wdguo@uow.edu.au

Tel: (61-2) 4221 3036

Number of tables: 4

Number of figures: 21

Words: 9642

References: 44

Key words: piles, closed-form solutions, soil movement, soil-structure interaction

Response of rigid piles during passive dragging

Wei Dong Guo

School of Civil, Mining and Environmental Engineering, The University of Wollongong, Australia
Tel: (61-2) 42213036 Email: wdguo@uow.edu.au; camsaweidguo@gmail.com

ABSTRACT

This paper develops a 3-layer model and elastic solutions to capture nonlinear response of rigid, passive piles in sliding soil. Elastic solutions are obtained for an equivalent force per unit length p_s of the soil movement. They are repeated for a series of linearly increasing p_s (with depth) to yield the nonlinear response. The parameters underpinning the model are determined against pertinent numerical solutions and model tests on passive free-head, and capped piles. The solutions are presented in non-dimensional charts, and elaborated through three examples. The study reveals the following:

- On-pile pressure in rotationally restrained, sliding layer reduces by a factor α, which resembles the *p*-multiplier for a laterally loaded, capped pile, but for its increase with vertical loading (embankment surcharge), and stiffness of underlying stiff layer: $\alpha = 0.25$ and 0.6 for a shallow, translating and rotating piles, respectively; $\alpha = 0.33–0.5$ and $0.8–1.3$ for a slide overlying a stiff layer concerning a uniform and a linearly increasing pressure, respectively; and $\alpha = 0.5–0.72$ for moving clay under embankment loading.
- Ultimate state is well defined using the ratio of passive earth pressure coefficient over that of active earth pressure. The subgrade modulus for a large soil movement may be scaled from model tests.
- The normalised rotational stiffness is equal to 0.1–0.15 for the capped piles, which increases the pile displacement with depth.

The 3-layer model solutions well predict nonlinear response of capped piles subjected to passive loading, which may be used for pertinent design.

Key words: passive piles, analytical solutions, non-linear response, soil-structure interaction, examples

1. INTRODUCTION

Vertically loaded piles may be subjected to lateral spreading (in the event of an earthquake). The piles are referred to as passive piles, as with slope stabilizing piles, and piles adjacent to an excavation or embankment (referred to embankment-piles later on). Their design entails incorporating the impact of sliding depth, pile-soil relative stiffness, rotational constraints (e.g. from pile cap, base, or even soil movement), and possible dragging [1-2].

Elastic solutions are deduced to simulate response of slope stabilising piles using measured thrust and gradient of soil movement with depth either a uniform [3] or an inverse triangular shape [4]. They are compelled to be coupled with magnitude of the soil movement, as with other methods [5-8]. The movement is converted into a fictitious concentrated load, with which the solutions for a laterally loaded pile is employed to capture nonlinear response of passive piles for each movement [9]. Nevertheless, 'flexible' piles turn to 'rigid' during lateral spreading, for which use of the concentrated load is not sufficiently accurate. To model the response of the rigid piles, Guo and Ghee [10] developed a new shear apparatus [see Figure 1(a)] and have conducted extensive tests on 'rigid'piles in moving sand. As discussed at length in this paper, Guo [11] further developed elastic solutions for rigid piles in 2-layer soil (with an upper sliding layer and a lower stable layer), and proposed to use the solutions together with stepwise uniform pressures to capture the impact of soil movement on nonlinear response of the piles.

Response of lateral piles is dominated by net limiting force per unit length, which is denoted herein as p_s for a passive pile due to soil movement, and as p_u along a laterally loaded (active), single pile [12]. The soil movement w_s exceeding w_s^* (= p_s/k_s, k_s = modulus of subgrade ration of sliding layer) induced the p_s over a depth l_m. It also exerts rotational restraint (acted as a thick, pile-cap) on free-head piles [9]. This resembles conditions on laterally loaded, rotationally restrained piles. The latter is associated with a reduced limiting force per unit length of αp_u (with α = 0.25−1.0) due to pile-pile interaction [13], or the pile cap-rotational constraint [12]. The ratio of 0.25, interestingly, is identical to the ratio of load on a fully fixed-head pile over that on a free-head pile at a given (elastic) head-displacement [9]. The limiting force per unit length p_s for passive piles, thus should reduce to αp_u as well with α = 0.25−1.0 [9], but for the impact of soil movement profiles, underlying stiff layer and vertical and/or embankment loading.

Numerical analyses on passive piles have produced useful results [14-17] by stipulating a correct value of p_s [9], e.g. $p_s = (2.8–4)s_u d$ for piles in sliding clay (s_u = undrained shear strength of clay, d = pile outside diameter or width) [8, 11, 18], which implies α = 1/3 due to p_{u1} =

(9.1−11.9)$s_{u1}d$ (for laterally loaded piles) [19] [11]. Without explicitly acknowledging these discrepancies, a direct use of p–y curves (for lateral piles) to model passive piles has incurred inconsistent predictions [20-22], and deduced p_s values mutated by an order of magnitude for piles in liquefied sand [23]. For instance, 2−layer numerical solutions were obtained for ultimate state [24], in which a linear increasing limiting force per unit length p_s (= $A_r z$, A_r = gradient for laterally loaded piles) with depth z is fully mobilised along passive piles. The parameter A_r used (with α = 1), however, is inconsistent with α = 1/3 for piles in clay. It offers, in fact, consistently ~67% higher maximum shear force T_m (thus bending moment M_m) than 3−layer model solutions (as developed later). Given a specified ultimate bending capacity (= M_m), a slope-stabilising pile would only take 60% (= 1/1.67) the T_m calculated. The associated factor of safety (FS), for instance, may reach 2.5 for a design value of 1.5 [16]. On the other hand, if total sliding thrust is shared using the maximum shear force (thrust) taken by each pile, 60% less number of piles may then be installed, which may compromise the safety. A reduced gradient of 0.6A_r (i.e. α = 3/5), as shown later, perhaps should be adopted to remove the ambiguity.

To tackle the inconsistency and ambiguity among available solutions, a 3-layer model and solutions are developed in this paper. The model is formulated by inserting a new layer in-between the upper sliding layer and the lower stable layer. The sandwich layer has a modulus increasing linearly from the upper k_s to the lower layer mk_s. Elastic solutions for the 3-layer model are developed and presented in non-dimensional expressions. They are adopted to gain non-linear response of the piles through applying a series of limiting force per unit length p_s. The input parameters (i.e. m, k_s, and p_s) underpinning the 3-layer model were determined by 'matching' with finite element method (FEM) simulation of piles in sliding sand overlying sand or soft rock, respectively. The cap rotational stiffness k_θ is determined using typical model tests. The impact of dragging and rotational stiffness on passive piles are examined against laterally loaded, capped piles, which reveals the evolution rules of the p_s (via the factor α), the modulus ratio m at design and ultimate states (defined using coefficients of earth pressures), and subgrade modulus k_s (at large soil movement). Ad-hoc guidelines are formulated for determining the input parameters. Finally, the solutions are elaborated, respectively, to capture nonlinear response of free-head piles, and 2-pile in-line groups in sliding sand, and embankment-piles in a clay-sand layer.

2. 3-LAYER MODEL AND SOLUTIONS

A pile is classified as rigid, once the pile-soil relative stiffness, E_p/G_{av} exceeds $0.052(l/r_o)^4$, as with a laterally loaded free-head pile [25-26]. Note that E_p = Young's modulus of an equivalent solid

pile; r_o = outside radius of a cylindrical pile; and G_{av} = average shear modulus over the pile embedment l.

The 2-layer model [11] is recaptured first herein to facilitate the development of the new 3-layer model. The pile-soil interaction under active or passive loading is modelled by a series of spring-slider elements distributed along the pile shaft [26] [see Figure 2(a)]. The soil movement w_s is encapsulated as an external, **l**inearly **i**ncreasing **f**orce **p**er **u**nit **l**ength with **d**epth [LIFPULD] p_s over the sliding depth l_m on the pile [see Figure 2(b) [27]]. This p_s is divided into a series of stepwise increased uniform p_s. The model is underpinned by the following stipulations:

- The spring has a subgrade modulus k_s and mk_s for the moving and the stable layer, respectively.
- The spring has a LIFPULD p_s (= $p_{ub}z/l$, p_{ub} = limiting force per unit length at a free-head, pile base, via the slider) increasing with depth z. As with the limiting force per unit length p_u along active piles [26], the p_s reduces with rotational stiffness k_θ [12].
- Impact of soil movement is mimicked by the LIFPULD p_s [= $\alpha p_{ub}l_m/l$] using increasing sliding depth l_m. It is adjusted by the factor α, which depends on soil movement profile (other than uniform), loading distance [from pile(s)] and rotational restraint on pile(s).

Critically important is that the pile response is calculated for elastic interaction (via the modulus k_s and m) under a uniform force per unit length being equal to the limit p_s (for the soil movement) over the sliding depth l_m [see Figure 2(e)]. A series of increasing uniform p_s (= $\alpha p_{ub}l_m/l$) are assigned [by gradually increasing the l_m (< the real sliding depth)] to calculate the associated elastic response. The 'elastic response' together constitutes the nonlinear response of the piles (as illustrated later on). It is novel to apply the force per unit length of p_s to enforce the upper plastic limit, and to increase gradually the p_s (together with l_m) to gain non-linear interaction. The reduction in the p_s with increasing rotational constraints is exemplified in Figure 2(b) for free-head (rotating) and fixed-head (translating) piles. The solutions also reveal that a uniform or a triangular profile of on-pile pressure [28-29] may be induced along lightly head-restrained or fully base-restrained piles, respectively.

2.1 3-layer Model

Rigid passive piles are largely simulated as embedded in a 2-layered soil [8, 11, 27], with an upper moving layer of thickness l_m [see Figure 2(c)]. Model tests [see Figure 1(a)] indicate the on-pile p(z) profile on a passive pile to the depth z_m [≈ 0.45–0.55 m] of maximum bending moment resembles that along the entire length of a laterally loaded pile [9]. Below the depth, the p(z) profiles under passive loading all have an additional portion, which vary approximately linearly from the negative $p(z_m)$ at $z = z_m$ to the positive $p(l)$ at the pile-base. The modulus thus varies accordingly with depth.

It is simplified herein as 3-layers, see Figure 2(d), a subgrade modulus k_s in depth $0 - l_m$ (the upper layer), a linearly increasing modulus from the k_s at depth l_m to mk_s at depth z_m (the transition layer), and a modulus mk_s in depth $z_m - l$ (the lower layer), respectively.

Given the simplified modulus profile, a 3-layer model and the associated solutions are established for a uniform p_s over a sliding depth l_m. Under a uniform p_s (an external loading) for the movement w_s*, the pile rotates rigidly to an angle ω_r and a mudline displacement w_g. The pile has a linear displacement $w(z)$ (= $\omega_r z+w_g$) with depth z, and a rotation depth z_r (= $-w_g/\omega_r$) at which $w(z_r)$ = 0 [see Figure 2(c) and (e)]. The on-pile force per unit length $p_i(z)$ [FL^{-1}] is proportional to the modulus of subgrade reaction k_s (= kd, k = a constant), and the local displacement $w(z)$. It is given by [see Figure 2(d)]: $p_1(z) = k_s w(z)$ in sliding layer (i = 1), $p_2(z) = k_s w(z)[1+(m-1)(z-l_m)/(z_m-l_m)]$ in transition layer (i = 2), and $p_3(z)= mk_s w(z)$ in stable layer (i = 3), respectively. The net on-pile resistance force per unit length $p(z)$ [FL^{-1}] is given by: $p(z) = p_1(z)-p_s$, $p(z) = p_2(z)$, and $p(z)= p_3(z)$ for the associated layers, respectively. The k_s is equal to $(2.2–2.85)G_{s1}$ (G_{s1} = shear modulus of the sliding soil), for instance, for model piles having l = 0.7 m, and d = 0.05 m [26]. The passive pile, see Figure 2(e), may be subjected to a head constraining-moment M_A, a base constraining-moment M_B, a lateral shear force H at head level, under the impact of a non-uniform soil movement and pile-pile interaction (i.e. p_s). The constraining moments M_A (= $k_A\omega_r$), and M_B (= $k_B\omega_r$) are modelled by the rotational stiffness k_A and k_B [30-33], and the impact by the factor α (e.g. α = 0.72 for an inverse triangular soil movement profile [27]).

It is stressed here that once the soil movement w_s exceeds the limiting displacement w_s* of p_s/k_s, the force per unit length $p_1(z)$ in sliding layer stays at the p_s, and is independent of movement profile; otherwise below the transition depth (with $w_s < w_s$*), the resistance $p_i(z)$ only relies on the local (elastic) pile displacement. Soil movement profile affects the transition depth only.

2.2 Model Solutions and Features

2.2.1 Elastic Solutions

The pile-displacement at depth z, $w(z)$ (= $\omega_r z+w_g$) is recast into

$$w(z) = (\overline{\omega}_r \overline{z} + \overline{w}_g) p_s / k_s \qquad (1)$$

where $\overline{\omega}_r$ [= $w'(z)k_s l/p_s$], $\overline{w}_g$ (= $w_g k_s/p_s$), and $\overline{z} = z/l$. The 3-layer model for the passive pile-soil system under the external loading p_s was resolved using Equation (1), the force equilibrium of, and bending moment about the pile, and the pile-soil displacement compatibility [see Figure 2(f)]. The derivation resembles that elaborated previously for the 2-layer model [11], which is not reiterated herein. Instead, the solutions are provided directly in Table I, involving the normalised mudline

displacement and rotation angle of the pile. For instance, the net force per unit length $p_2(z)$ on the piles in the transition layer is described by

$$p_2(z) = (\overline{\omega}_r \bar{z} + \overline{w}_g)[(m-1)\frac{\bar{z} - \bar{l}_m}{\bar{z}_m - \bar{l}_m} + 1]p_s \tag{2}$$

where

$$\overline{w}_g = \frac{-6(1+\bar{z}_m)(\overline{H} + \bar{l}_m)}{(m-1)(-2\bar{l}_m^2 + \bar{z}_m\bar{l}_m + 3\bar{l}_m + \bar{z}_m^2) - 3(1+m)\bar{z}_m} \tag{3}$$

$$\overline{\omega}_r = \frac{12(\overline{H} + \bar{l}_m)}{(m-1)(-2\bar{l}_m^2 + \bar{z}_m\bar{l}_m + 3\bar{l}_m + \bar{z}_m^2) - 3(1+m)\bar{z}_m} \tag{4}$$

where $\bar{l}_m = l_m/l$, normalised sliding depth, $\overline{H} = H/(p_s l)$, normalised lateral shear force (at head-level); and $\bar{z}_m = z_m/l$, normalised depth of maximum bending moment, which is given by

$$\bar{z}_m^2 + \overline{B}\bar{z}_m + \overline{C} = 0 \tag{5}$$

where

$$\overline{B} = \frac{3 + [3(1+m) + \bar{l}_m(1-m)]\overline{C}_1}{(1-m)\overline{C}_1} \tag{6a}$$

$$\overline{C} = \frac{m - (m-1)\bar{l}_m[3(\overline{C}_1 + 1) + \bar{l}_m(\bar{l}_m - 2\overline{C}_1 - 3)]}{(1-m)\overline{C}_1} \tag{6b}$$

$$\overline{C}_1 = \frac{\bar{k}_\theta\overline{\omega}_r + \overline{H} + \bar{l}_m(1 - 0.5\bar{l}_m)}{-(\overline{H} + \bar{l}_m)} \tag{6c}$$

where $\bar{k}_\theta = k_\theta/(k_s l^3)$, normalised rotational stiffness; and k_θ is the total rotational stiffness along the pile, including the top k_A and the tip restraining stiffness k_B (e.g. from non-liquefied layer) in Figure 2(e). The stiffness k_A and k_B may have different values, but the associated angle of rotation ω_r is identical along the pile. The $\bar{z}_m$ is calculated iteratively using Equation (5) and the $\bar{k}_\theta$-dependent coefficients $\overline{B}$ and $\overline{C}$, or directly estimated (without iteration) using Equation (5) at $\bar{k}_\theta = 0$. This can be readily fulfilled using modern mathematical software (e.g. Mathcad ™), as illustrated later for free-head ($k_A = k_B = 0$) and capped piles ($k_A \neq 0$).

2.2.2 Salient Features

The explicit expressions in Table I encompass normalised shear force $T_i(z)/(p_s l)$, normalised bending moment $M_i(z)/(p_s l^2)$ and on-pile force per unit length $p_i(z)$ for the upper, the transitional, and the lower (stable) layer, respectively. They allow estimation of normalised maximum bending moment $M_{m2}/(p_s l l_m)$ and shear force $T_{m3}/(p_s l)$ [M_{m2} and T_{m3} = maximum of $M_2(z)$ and $T_3(z)$]. It should be stressed that (1) the net force per unit length in sliding layer $p(z)$ is the difference between the on-pile $p_1(z)$ and the 'external' p_s; (2) An increase in the rotational stiffness k_θ (via $k_A = k_\theta$)

renders the depth z_m advance towards the pile base ($z_m \rightarrow l$), until the stable layer vanishes; (3) A relatively large sliding depth l_m renders the two depths z_m and l_m converge together (and the 3-layer reduces to 2-layer); (4) The sliding depth l_m is measured at the pile location, otherwise it is taken as c (= l_m/β, β >1); (5) With rotational restraint lumped at the pile-head ($k_\theta = k_A$) or the base ($k_\theta = k_B$), the net pile displacement with depth should be calculated as $w(z)+\lambda_d z M_m/k_\theta$ or $w(z)+\lambda_d(l-z)M_m/k_\theta$, respectively, in which $\lambda_d = 0.667$ for a LIFPULD p_s with depth ($\lambda_d = 0.5$ for uniform p_s). (6) The non-dimensional response such as $\overline{\omega}_r$ and $\overline{w}_g$ depends on m, $\overline{l}_m$, $\overline{H}$, and $\overline{k}_\theta$ as with the $\overline{z}_m$. The soil movement of p_s/k_s comes into play only in gaining the dimensional response.

2.2.3 Equivalent p_s (Limiting Loading)

The 3-layer model solutions for a single pile is readily applied to piles in groups by employing reduced moduli of $p_m k_s$ and $p_m m k_s$ (by a multiplier p_m<1, to cater for the pile-pile interaction) and reduced LIFPULD of αp_s (by the factor α). The external p_s can be of any distributions (e.g. increasing to the power of depth). Guo [12] demonstrates that it is adequate to use uniform and LIFPULD p_u profiles (with depth) to model active piles in clay and sand (stiff clay), respectively. As the problems addressing here are generally pertinent to sand or clay with sufficient strength, the p_s due to moving soil is stipulated as linearly increase with depth. It is proportional to the factor α ($\approx w_g/w_s$) due to elastic interaction. The external p_s is thus described by

$$p_s = \alpha p_{ub} l_m / l \qquad (7)$$

where p_{ub} is the force per unit length at base level of a passive pile; and l_m is the sliding depth at loading position (except where specified). The parameters p_{ub} and α are ascertained in the next section, for rotating (of free-head, $k_\theta = 0$), and translating (of fixed-head, $k_\theta > 10E_pI_p$, E_pI_p = flexural stiffness of a pile[12]) piles, respectively, although fixed-head piles may rotate as well at $l_m > 0.5l$. The accuracy of the 3-layer model together with Equation (7) is illustrated later through comparison with FEM analysis of slope stabilising piles, and embankment piles, respectively. It should be stressed that the solutions are contemplated for rigid piles with free-displacement at pile base, otherwise the previous solutions [2, 34] should be consulted.

2.3 Determination of Model Parameters

Study to date [11, 27] indicates that with a large, sliding movement, the parameters p_{ub}, m, k_s, α and c may be determined using the ad-hoc guidelines G1-G7.

G1: A loading depth l_m [at a distance $0.7l$] enforces an actual loading depth c [= l_m/β, β= 1.0–1.4] at the pile location.

G2: The limiting force per unit length at pile-tip level p_{ub} (of a free-head, single, passive pile) may be estimated using G2a–G2c for the associated α at $P = 0$ or $q = 0$ (otherwise see G4).

- **G2a**: p_{ub} = (9–12)$s_u dl$/c for a deep sliding, clay layer ($l_m > 0.5l$), incurred by mobilization of the limit p_s of (3–4)$s_u dl$/c to the loading depth c (along with α = 1/3); p_{ub} = (1–1.4)(9–12)$s_u dl_m$/c for a shallow depth of sliding clay overlying stable sand layer (with α = 0.33–0.6), with the resistance being increased by ~ 40% [25, 35], as noted in numerical analysis on active piles.
- **G2b**: p_{ub} is calculated as $s_g \gamma' K_p^2 dl$ for piles in sliding sand, involving unit weight γ′(effective) and angle of internal friction ϕ for sand over the pile embedment [25, 36]. s_g incorporates installation effect, with an average s_g of 1.29 [9] (with α = 0.25–0.6, for $P = 0$ and $l_m < 0.5l$).
- **G2c**: p_{ub}/d is taken as the overburden stress at the pile-tip (i.e. identical to G2b at $K_p = 1$), as with that employed for piles subjected to lateral spreading [28-29, 37].

G2a and G2b are purported for a sliding soft clay, and sand layer, respectively, whereas G2a and G2c are for a shallow, moving clay overlying a sand layer [27].

G3: The limiting force per unit length reduces by a multiplier factor p_m due to pile-pile interaction, as with the p_m given for laterally loaded piles [9]

$$p_m = 1 - a(12 - s/d)^b \qquad (8)$$

where s is pile center-to-center spacing; $a = 0.02+0.25Ln(n_r)$; $b = 0.97(n_r)^{-0.82}$, n_r = row number. The p_m may be taken as the factor α (see G4) to further incorporate the impact of soil movement.

G4: The limiting force per unit length p_{ub} reduces to p_b (= αp_{ub}). The α value is dominated by the interplay among the p_s profile, the rotational restraint, and the vertical load P (or embankment surcharge q). The α value in G2 needs to be checked against the following:

- **G4a**: Single, free-head piles ($l_m < 0.5l$): (i) α = 0.25–0.6 (norm) for undefined sliding interface ($m = 1$) and $P = 0$; (ii) p_{ub} ($P \neq 0$, or $q \neq 0$) = ~ $1.5p_{ub}$ ($P = 0$ or $q = 0$) noted in model tests [see p(z) profiles]; and (iii) $\alpha \approx w_g/w_s$, the ratio of pile displacement over soil movement w_s.
- **G4b**: Capped piles: α = 0.25–0.6, and α = 0.25 for translating piles at $l_m < 0.5l$, otherwise α ≈ 0.6–1.0 for deep sliding and $P \neq 0$.
- **G4c**: The force per unit length p_s in a moving clay may be induced by embankment surcharge q [11], and is governed by $p_s = \alpha dq$ with α = 0.50– 0.72. The higher α values than norm include the increasing impact of the surcharge and underlying stiff layer.

Model tests and numerical analysis indicate that (a) The limiting p_{ub} can only be mobilised at a sufficiently high rotation of the piles; and it drops to the lowest limit of $0.25p_{ub}$ for translating piles (normally with a uniform pressure p_s). (b) The p_s may increase by ~40% due to underlying stiff

layer (m >1), and by ~50% due to vertical load P or embankment surcharge q (but with a reduced m, see G5). A stiff layer (m > 1) may render α increase to 0.33–0.35 [= 0.25× (1.3–1.4)] (2-layer clay), and 0.8–0.84 [= 0.6×(1.32–1.4)] (2-layer sand), respectively; and further to 0.5–0.53 [= 1.5×(0.33–0.35)], and 1.2–1.3 [= 1.5×(0.8– 0.84)] due to loading P and/or q, for translation and rotational movement, respectively. These α values agree well with available data [27].

With a loading distance of 0.7l and a sliding depth of 0.286l, as shown in a later example, the force per unit length p_s is taken as $(\alpha p_b)(c/l)$ with $\alpha = 0.6$ in predicting profiles of on-pile response.

G5: The modulus ratio m (= k_{s2}/k_s) is ratio of the subgrade modulus of underlying (stable) layer k_{s2} over that of an upper, moving layer k_s. The ratio at 'ultimate state' is taken as K_{p1}/K_{a2} [K_{p1}, and K_{a2} = coefficients of passive earth pressure (sliding layer) and active earth pressure (stable layer), respectively]. This newly defined 'ultimate state' is comparable with the 'ultimate state' for reaching limiting pressures in sliding and stable layer for piles in clay [8] or sand [24], respectively.

- **G5a**: $m = K_{p1}/K_{a2}$ (ultimate state at a large soil movement) e.g. m = 17.7 for $\phi = 38^o$.
- **G5b**: m = (0.6–0.7)K_{p1}/K_{a2} (Design-level soil movement), pertaining to non-dragging from the underlying sand layer (associated with a limited vertical load P) and/or $l_m > 0.5l$, for instance, m (Design level) = 10–13 for $\phi = 38^o$ [25].
- **G5c**: $m = 2.1K_{p1}/K_{a2}$ for a sliding sand overlying a stable, soft rock.

G6: Unless provided, the modulus of subgrade reaction k_s for a sliding sand layer may be estimated by

$$k_s = 51d\lambda \frac{K_{p1}}{K_{a2}} \left(\frac{l_{2c}}{l_m} \right)^2 \frac{p_{u2}}{p_{u1}} \qquad (9)$$

where d in m, k_s in kPa, λ (= 1–3) is modification factor, high value for short piles; l_{2c}/l_m = 1–1.3($l_m < l/3$) and $l_{2c} = l_m$ ($l_m > 0.5l$); and $p_{u2}/p_{u1} \leq 3$ (p_{u1}, p_{u2} = limiting force per unit length for a passive pile in the sliding and the stable layer, respectively). Equation (9) assumes the k_s is proportional to the diameter and the coefficient K_{p1} [26]. It is purported for a large deformation (typically > 0.5 m) and small k_s, regardless of the soil properties. It should be stressed that

- The k_s, for instance, for a model pile (d = 0.05 m) in sand ($\phi = 38^o$) was deduced as ~ 45 kPa during passive loading [38].
- The k_{s2} for a moving sand layer underlying a sliding clay layer (beneath an embankment) may also be estimated using Equation (9). For instance, the modulus k_{s2} [39], for an embankment pile with d = 430 mm, is estimated as ~387 kPa (= 45×430/50, at $\phi = 38^o$). This in turn allows k_s of the overlying clay layer to be estimated as ~22 kPa (= ~387/m, m = 17.7). The associated prediction compares well with measured pile response (not shown herein).

- The k_s gained using Equation (9) is consistent with these deduced from typical piles subjected to lateral spreading [40-41], such as k_s = 25.2−72 kPa (Pile No.1, Niigata FCH Building), k_s = 64 kPa (PC-pile building in Higashi-Nada, Kobe), and k_s = 23 kPa (Tank TA72 at Mikagehama Island); and
- The incorporation of the non-dimensional parameters l_{2c}/l_m, p_{u2}/p_{u1}, and λ into the k_s of Equation (9) is based on numerical solutions as presented later.

G7: The normalised rotational stiffness $\bar{k}_\theta$ is less than 0.3 for the capped model tests in Figure 1 [42], which will be discussed late and at length elsewhere.

The ad-hoc guidelines G1−G7 are synthesized from good predictions of nonlinear response of four model piles in sliding soil, one in-situ test pile in a sliding embankment, six centrifuge tests on piles subjected to lateral spreading [27], and three centrifuge tests on piles adjacent to embankment.

2.4 Comments on 3-layer Model ($k_A = k_B = 0$, and $H = 0$)

Both 3-layer and 2-layer model solutions warrant force equilibrium of, moment equilibrium about the pile and pile-soil displacement compatibility (thus rigorous) under the 'external' p_s. The 2-layer model solutions are readily obtained (without iteration in calculating the depth of maximum bending moment z_m), and are sufficiently accurate for modelling those piles in sliding slope or subjected to lateral spreading (without dragging) [27]. The model, however, overestimates the shear force (thus bending moment) by ~67% for progressive movement with dragging. The new 3-layer model reduces to the 2-layer model at a large sliding depth (with $z_m = l_m$). It retains the features of the 2-layer model but with better accuracy for more wide problems, as highlighted next for piles in clay and sand, respectively.

2.4.1 Uniform p_{u1} (or p_s)

Viggiani [8] developed a 'ultimate-state' solution for passive piles in two-layered clay assuming a limiting resistance per unit length p_{ui} (= $k_i s_{ui} d$) in sliding layer (i = 1) and stable layer (i = 2), respectively. The correlation factor k_1 is equal to 3−4 [= (9.1−11.9)α, and α = 1/3], as mentioned in G2a, G4b and p_{ui} [= (9.1−11.9)s_{u1}] [19]. With the solution, the maximum shear force (or thrust) T_m (at the sliding depth l_m) and maximum bending moment M_m in the piles were estimated and normalised by p_s (= 3.33$k_1 s_{u1} d$, for convenience). The normalised thrust $T_m/(p_s l_m)$ agrees with that obtained the 2-layer (elastic) model [11] (see Figure 3), as is evident for m = 1.5, 3 and 5 (with l_m/l = 0−1), respectively. Using the new 3-layer solutions for m = 3, 5, 10 and 15, the normalised force was obtained and is plotted in Figure 3(a) as well. Its difference from those obtained using the 2-layer model [e.g. for m = 3, and 5] is the normalised dragging resistance. The values of the moment

M_m at l_m (2-layer model) and that at z_m (3-layer) were calculated and normalised as $M_m/(p_s l l_m)$. As shown in Figure 3(b) (m =1−10), the 2-layer and the 3-layer models offer barely discernable curves of $T_m/(p_s l_m)$ versus $M_m/(p_s l l_m)$ at $-M_m/(p_s l l_m) < 0.1$. The ratios of $T_m l/M_m$ (i.e. the gradient of the curves) fall within 2.5−6 (thin, solid lines) gained from field and laboratory tests on piles in sliding soil or adjacent to excavation [38]. Given a bending capacity, the 2-layer and 3-layer models offer similar resistance T_m, but the former offers a ~20% deeper sliding depth [see Figure 3(a)]. This implies that any over-design or under-design using 2-layer model is largely incurred by using the larger gradient of limiting force proposed for laterally loaded piles.

2.4.2 LIFPULD p_{u1} or p_s

Given a LIFPULD p_s (=$A_r z$, as observed along piles in sand or stiff clay), normalised sliding thrust of $T_m/(p_s l_m)$ (p_s= $0.5A_r l_m$ and A_r= $3\gamma' K_{p1} d$) in piles at 'ultimate state' was obtained numerically [24] for K_{p2}/K_{p1}=1, 2 and 3, respectively at the full spectrum of normalised sliding depth l_m/l. The thrust was estimated using the 2-layer (elastic) solutions by taking $m = K_{p1}/K_{a2}$, $2K_{p1}/K_{a2}$ and $3K_{p1}/K_{a2}$, respectively (see Case I in Table II). It was normalised by $p_s = 0.37A_r l_m$ (= $0.5\alpha A_r l_m$, α = 0.74) to match the 'ultimate-state' values [see Figure 4(a)]. The factor 'α = 0.74' implies that the ultimate-state solutions have a p_s 35% higher than the 2-layer solutions. The shear force (thrust) was also obtained using the 3-layer solutions, and normalised to match the ultimate solutions [see Figure 4(b)] by taking $p_s = 0.3A_r l_m$ (= $0.5\alpha A_r l_m$, α = 3/5). The comparison warrants using a reduced gradient of $0.6A_r$ for a LIFPULD p_s, as with the pressure of $(9-12)\alpha s_u$ (α = 1/3) for a uniform p_s. The gradient of $A_r = 3\gamma' K_{p1} d$ [24, 43] adopted for active piles should be reduced to A_r (= $1.8\gamma' K_{p1} d$) [24, 43] once soil movement (passive loading) is inflicted.

2.5 Nonlinear Response

The 3-layer (elastic) solutions are employed to gain nonlinear response by increasing l_m and p_s [via Equation (7)], as with 2-layer model [11, 27]. Note the l_m is measured at pile location [see G1 and G4, otherwise reduced, e.g. to $(0.7-1)l_m$ for SD= $0.286l$, at a loading distance of $0.7l$]. Assuming a uniform p_s to a sliding depth c of $il_m/50$ [l_m = a final sliding depth (SD) estimated from slope analysis, or simply taking l_m = $(0.7-0.9)l$], calculation is repeated for step i = 1, 2, .., 50, respectively. The envelope of the stepwise increased uniform p_s (applied) gained from Equation (7) becomes a triangular profile of p_s [see Figure 2(f)].

The z_m is determined using Equation (5) for a desired l_m, which in turn allows the normalised displacement $\overline{w}_g$ and rotation $\overline{\omega}_r$ to be calculated using Equations (3) and (4),

respectively. The z_m is substituted into $M_2(z)$, $p_i(z)$, and $T_i(z)$ (see Table I) to gain the maximum bending moment M_m, the net on-pile force per unit length $p(z)$, and shear force $T(z)$, respectively. The pile response at a loading depth c is estimated by taking l_m = c in the expressions and the on-pile force per unit length p_s, which encompasses the magnitude and the depth of M_m, the maximum shear force T_m in a pile under each p_s for a set of five parameters k_s, m, k_θ, p_b and α. Conversely, the factor α may be deduced from the measured ratio of the movement w_s over the pile displacement w_g; the values of k_s, m, p_b and k_θ from measured rotation angle, displacement and bending moment (at a typical sliding depth), and the measured profile of on-pile force per unit length; and finally, the loading depth c from measured 'ultimate' profile of bending moment. The calculation steps are adopted for all later predictions or back-estimations against measured data.

It is worth to mention that the profile of effective soil movement w_s*(= p_s/k_s) for Equation (7) follows the same triangular [in Figure 2(a)] shape of the p_s (applied), regardless of the uniform p_s over the depth l_m for each step. It induces an inverse trapezoidal shape of on-pile force per unit length p(z) along an in-situ slope stabilising pile ($H \neq 0$ at pile head) [21]; and a parabolic p(z) with depth along the head-restrained ($k_\theta \neq 0$) piles subjected to lateral spreading [28]. A low limit w_s is observed for $\alpha < 1$ (with a reduced p_s).

3. PARAMETERS FOR k_s AND FEM ANALYSIS

Numerical (FEM) analysis was conducted [43], respectively, on the piles embedded in stable layer of (a) loose sand with ϕ (angle of internal friction)= 28°, ψ (angle of dialatancy) = 2°, c (cohesion)= 3 kPa, and G_{s2} (shear modulus) =16 MPa (Case II, Table II); (b) Dense sand with ϕ = 38°, ψ = 2°, c = 3 kPa, and G_{s2} = 32 MPa (Case III); or (c) Soft rock with ϕ = 45°, ψ = 5°, c = 50 kPa, and G_{s2} = 1.2 GPa (Case IV). The piles (d = 1.2 m) were subjected to a 6 m-thick, sliding layer of loose sand (ϕ = 28°, ψ = 2°, c = 3 kPa), overlying the stable layer (a), (b) or (c) of 4.2, 6.0, 7.2 or 9 m in thickness, respectively. The ratio of the limiting force per unit length p_{u2} (stable layer) over the p_{u1} (sliding layer) was taken as 1, 1.6, and 3, respectively. The numerical simulations offer displacement w_g or maximum bending moment M_m versus resistance, which are re-plotted in Figures 5, 6 and 7, respectively.

The 2-layer solutions [i.e. 3-layer solutions (at $l_m = z_m$) without dragging] were obtained (by the procedure highlighted early using a series of depths) to match the nonlinear moment M_m and displacement w_g for each of typical sliding layer l_m (= 0.4l, 0.45l, 0.5l and 0.588l) of Cases II, III and IV, respectively. The 'match' with the numerical results renders p_{u2}/p_{u1} = 1−3, l_{2c}/l_m = 1−1.3, and λ = 1−3 in Table II, which are incorporated into the guidelines (e.g. G5 and G6) outlined

previously. The match, however, ignores the difference at a large sliding depth (> 0.5*l*) that maximum bending moment (at the maximum thrust) drops continuously in the current solutions (see Figures 5–7). The 'drop' trend is not observed in the numerical solutions despite that it is evident in the measured moments and head-displacements of piles subjected to lateral spreading [32], or embankment loading [21]. Note the available *M*(z) profiles of a few piles (Case III) are also well predicted against the numerical results (not shown herein).

4. PARAMETRIC ANALYSIS (*H* = 0)

4.1 Normalised Elastic Solutions

The 3-layer solutions were utilised to examine the impact of the rotational stiffness k_θ and the modulus ratio *m* (dragging) on nonlinear response of the pile, as the impact of the parameters k_s, p_s and α is incorporated into the normalised (i) mudline displacement induced by a sliding movement, $\alpha w_g/w_s$ (see Figure 8); (ii) rotational movement of the pile $\omega_r k_s l/p_s$ (Figure 9); (iii) maximum bending moment $M_m/(p_s l_m l)$ at z_m and/or sliding depth l_m (Figure 10); and (iv) thrust $T_m/(p_s l_m)$ at sliding depth (Figure 11), and shear force $T_{m3}/(p_s l_m)$ in stable layer (Figure 12).

Figure 8 provides the increase in the normalised pile-head displacement, $\overline{w}_g$ with the normalised sliding depth, concerning the normalised rotational stiffness $\bar{k}_\theta$ [= 0–0.4, see Figure 8(a) for *m* = 10] and the modulus ratio *m* [= 1–21 for $\bar{k}_\theta$ = 0.1, Figure 8(c)]. As expected, it is identical between the 2-layer and the 3-layer models at *m* = 1 (a uniform modulus across the subsoil) [e.g. Figure 8(b)]. Figure 9 shows the normalised pile displacement $\overline{w}_g$ versus the normalised rotational displacement (= $\omega_r l$) $\overline{\omega}_r$ relationship. The extra displacement of $\overline{w}_g$ beyond unity somehow reflects the rotational component owing to dragging. This dragging component reduces (and vanishes eventually) with increase in $\bar{k}_\theta$ [e.g. for $\bar{k}_\theta \geq 0.2$ at *m* = 1 in Figure 9(a)], or increase in *m* [e.g. at $\bar{k}_\theta = 0.1$ and *m* = 21 in Figure 9(b)]. At a given normalised displacement, the 3-layer model predicts a high normalised rotation than the 2-layer model does.

The maximum bending moment M_m varies with the location of rotational restraint (e.g. pile-head, base, or sliding depth). The normalised bending moment, $M_m/(p_s l_m l)$, for a base restrained pile (i.e. $\bar{k}_B = \bar{k}_\theta$), was calculated and is plotted in Figure 10. The figures indicate that the dragging (from *m* = 1 to 21) generally doubles the moment 'M_m' at sliding depth l_m, but renders only ~5% variation of the moment M_m at the depth z_m (bottom of the transition layer). The normalised M_m at z_m, however, increases with the base rotational restraining stiffness, and approaches the upper limit

of 0.5 [see Figure 10(a)]. The condition of $\overline{w}_g > 1$ [in Figure 10(a)] renders two peaks of shear force T_{m1} (sliding layer) and T_{m3} (stable layer); otherwise with $\overline{w}_g \leq 1$, only one peak force exists. The normalised thrust $\overline{T}_m$ in stable or sliding layer at $m > 1$ (dragging effect) is different between the 2-layer (i.e. $\overline{T}_{m1}$ and $\overline{T}_{m2}$) and the 3-layer models (i.e. $\overline{T}_{m1} = \overline{T}_{m2}$, and $\overline{T}_{m3}$ for stable layer), but it is identical [see Figure 11(b)] for $m = 1$. The peak T_{m3} (and the stable layer, see late example) vanishes at $\overline{k}_\theta > 0.1$ and invisible in Figure 12(a) and (b). Restraining pile-head only (i.e. $\overline{k}_A = \overline{k}_\theta$), the impact of dragging on the moment is not pursued here, as it can be observed from later example predictions.

4.2 Comparison with Measured Data

Guo [11] estimated the ratio of $M_m/T_m l$ as 0.3–0.45 for a concentrated loading H (H-based model) at a depth l_m (= ~ 0.33l, H-based model), and for a uniform loading p_s over the sliding layer l_m (= ~0.5l, 2-layer model), respectively. As replotted in Figure 13, the $M_m/T_m l$ ratios bracket well 0.33–0.39 gained from the model tests on 'rigid' passive piles in sand [38] with $M_m/T_m l = 0.33$ (l_m = 0.57l) and 0.39 (l_m = 0.286l) for 50 mm-diameter piles and $M_m/T_m l = 0.35$ and 0.38 for 32 mm-diameter piles (see the next section). Both the H-based and the 2-layer models offer an $M_m/T_m l$ attenuating with increasing sliding depth ($\leq 0.5l$).

Assuming a normalised cap-rotational stiffness (Nor_$k_\theta = \overline{k}_\theta$) of 0, 0.1, 0.2 and 0.3, the $M_m/T_m l$ ratios were calculated using the 3-layer model for m = 7.67 (design state), or 17.7 (ultimate state) with soil frictional angle ϕ of 38°, and are plotted in Figure 13(b) together with the measured data [38]. The figure indicates that at a high normalised 'sliding' depth, the centrifuge test piles (denoted as 'Leung et al') [44] was indeed rotationally restrained (with $\overline{k}_\theta$ = ~0.2) by the 3 m away, front retaining wall (of the excavation). The restraining effect (with $\overline{k}_\theta$ = 0.1–0.3) is also deduced for the Kamimoku-4 and Kamimoku-6 piles, which is not explored here due to lack of the pile-slope detail.

5. MODEL TESTS OF PILES IN MOVING SAND

Model tests on piles in progressively sliding sand (see Figure 1) are simulated herein, which provide a standard case of k_s for Equation (9).

5.1 Model Tests under Uniform or Inverse Triangular Soil Movement

Model tests [38] were conducted using the shear apparatus in Figure 1(a) with 1×1 m^2 in plan and

0.8 m in height to simulate response of passive piles. An inverse triangular (T) [or a uniform (U)] loading block was applied laterally on aluminum frames of the upper portion of the shear box and translated. It presumably generates a T or a U profile of soil movement w_f [at the loading distance of 0.7l from the single piles, Figure 1(b_1), or from the center of 2-piles, Figure 1(c_1)], respectively, but an unknown sand movement profile around the pile. The model piles tested, referred to as d_{32} piles, were made of aluminum tube, 1,200 mm in length, which have d (outside diameter) = 32 mm, t (wall thickness) = 1.5 mm, and E_pI_p (calculated bending stiffness) = 1.28×10^6 kNmm^2. The sand of the model ground in the shear box had a unit weight of 16.27 kN/m^3, and an angle of internal friction ϕ of 38^o. The lateral block displaced the frames (thus the sand) to a maximum depth l_m at an increment of 10 mm (measured on the top frame), until a total frame movement w_f of 110–140 mm. The model sand was subjected to an overburden stress of 3.25–6.5 kPa (without surcharge on the surface), but for ~10% additional shear resistance from tested pile(s) installed in the shear box [38].

The T-block or U-block tests on the d_{32} piles (embedded to a depth of 700 mm in model sand) [38] are denoted by the associated letter T or U for block shape, and a second letter S or D for a sliding depth of 200 mm or 400 mm. Typical tests are simulated later, as elaborated next.

5.1.1 Five T-block Tests on Single Piles

Five tests of T32-0 series were conducted using the T-block on free-head d_{32} piles to a depth of 125, 200, 250, 300 and 350 mm, respectively [see Figure 1(b_1)], which provide (i) the ultimate on-pile pressure profiles with depth shown in Figure 14(a); (ii) The maximum bending moment M_m and rotational angle under various displacement w_g presented in Figure 14(b) and (c) respectively; (iii) The moment M_m versus the maximum shear force T_{mi} induced in the piles (for stable and sliding layers) drawn in Figure 14(d); (iv) The evolutions of the moment M_m and the shear force T_{mi} plotted in Figure 15(a) and (b) with the frame (soil) movement w_f [note the initial movement w_i (= 50 mm) causes negligible pile response]; (v) The variations of the moment M_m, the shear force T_{mi}, and the pile- displacement w_g with the sliding depth ratio R_L(= l_m/l) depicted in Figure 16(a), (b) and (c) [with an initial ratio R_i (= 0.05–0.15) associated with negligible pile response]. The M_m, T_m, w_g and the ultimate $p(z)$ are ascertained from profiles of bending moment $M(z)$, shear force $T(z)$, displacement $w(z)$ and on-pile force per unit length $p(z)$, which are exemplified in Figure 17 for the test TS32-0 at l_m = 200 mm.

5.1.2 Two U-block Tests on 2-pile in-line Groups

Tests US32-0 and US32-294 [see Figure 1(c_1)] were conducted on capped-head 2-piles (d_{32}) in line (at a center -to- center spacing of 3d) to a sliding depth of 200 mm using the uniform loading block,

with a load (P = 294 N per pile), or without the load (P = 0) on the pile-cap, respectively. The tests afford for pile A [close to loading block, Figure 1(c_1)], (i) the maximum bending moment M_{mi} (in the pile and at ground-level) versus pile displacement w_g curves shown in Figure 18(a); (ii) the profiles of (ultimate) on-pile force per unit length, p(z) in Figure 18(b); (iii) the response profiles of (ultimate) bending moment M(z), and shear force T(z) in Figure 18(c) and (d), respectively. And furthermore, (iv) the variations of the moment M_{mi} and the shear force T_{mi} with the frame movement w_f in Figure 19(a) and (b); (v) the pile deflection w(z) profiles in Figure 19(c_1) and (c_2); (vi) the moment M_m and M_o (at mudline) against the pile displacement w_g in Figure 19(d); (vii) the p(z) profiles in Figure 19(e); and (viii) the moment versus displacement curves, and the p(z) profiles for Pile B (see the inset in Figure 18), as an example, in Figure 19(d) and (e), respectively. A LIFPULD p_s with the sliding depth is observed for free-head piles, see the dash lines in Figure 14(a), to a sufficiently high rotation, which is not evident along capped piles in Figures 18(b) and 19(e) [42].

5.2 Modelling Free-head and Capped Piles

The current 3-layer model was used to simulate the measured response of the free-head, single piles, and the capped 2-piles [see Figure 1(b_1) and (c_1)]. The parameters are determined as follows:

- m =17.7 (= K_{p1}/K_{a2}, for ϕ = 38°), and m =13, reduced by 30–40% from 17.7 (G5) for limited mobilization of the resistance for no axial load P = 0, and/or without a dragging layer.
- The subgrade modulus k_s (of the sliding layer) was estimated as 50 kPa using Equation (9) in light of m =17.7, d = 0.032 m, l_{2c}/l_m = 1 (rigid piles), p_{u2}/p_{u1} = 1 (for the same sand in sliding and stable layer), and λ = 1.73. This k_s value agrees with 45–58 kPa gained using $k_s = 4.64p_{ub}$ [11] for the pile slenderness ratio and p_{ub} = 9.6 –12.5 kN/m [= (300–390)d, see Figure 14(a)]. It nearly doubles, as expected, the secant value of 25–35 kPa deduced from the pile bending moment [38]). The modulus k_s is equal to 50[1+(m-1)(z-l_m)/(z_m-l_m)] (transation layer) and 885 kPa (= mk_s, stable layer), respectively
- The p_{ub} was estimated as 10.0–11.6 kN/m using $p_{ub} = s_g\gamma' K_p^2 dl$ (see G2b), in which d = 0.032 m and l_m = 0.7 m (piles); γ' = 16.5 kN/m^3, and ϕ = 38° (sand layer); and s_g =1.53–1.77 (on high side to cater for jack-in installation of the piles [9]).

5.2.1 Free-head d_{32} Piles (T tests, α = 3/5 for P = 0)

The free-head pile tests were described by $k_A = k_B = k_\theta = 0$, and H = 0, without any 'lumped', rotational constraints other than the sand resistance. The 3-layer predictions were made using m/k_s(kPa)/p_b(kN/m) of 13/50/10 (Prediction I), 17.7/50/10 (Prediction II), respectively. They are based on p_{ub} (= p_b, and α = 1.0 at the pile location) for the displacement w_g, bending moment M_m,

and shear force T_{mi}. The predicted curves of w_g versus M_m, and w_g versus rotation ω_r (I and II) are plotted in Figure 14(b) and (c), respectively, which compare well with the measured data. The evolution of moment M_m and shear force T_{m2} (stable layer) (II) is also well predicted, as shown Figure 14(d) until l_m/l exceeds 0.3. This implies a good prediction for deep sliding at l_m/l = 0.7 −1.0 as well (as it is simulated as if l_m/l = 0–0.3 [27]). The 'Predictions I and II', however, overestimate the maximum shear force T_{m1} (sliding layer) by 30% for the current tests. As a comparison, the 2-layer prediction, using m/k_s(kPa)/p_b(kN/m) = 7−11/60/12.5 [27], also agrees well with the measured displacement w_g and moment M_m relationships [see Figure 14(b)].

An 'α = 0.6' is used to cater for impact of the loading distance of 0.7l from the piles (as per G4) concerning the loading depth c, movement w_f, and sliding depth ratio R_L, respectively.

(a) Pressure Profile: The profiles of on-pile pressure $p(z)/d$ were predicted for the loading depth c (= 0.82l_m, G1) at the pile location using p_s (= 6c/l, α = 0.6). They are plotted in Figure 14(a) for c = 82, 164, 246, 328, and 410 mm, respectively concerning l_m = 0.1, 0.2, 0.3, 0.4, and 0.5 m (at the loading location). Given k_θ = 0, H = 0, m = 13, and p_b = 1.74 kN/m (= 0.6×10×0.286), taking c = l_m = 0.2 m (i.e. l_m/l = 0.286) for instance, Equations (5) and (6) are resolved together to yield z_m = 0.352 m (which involves k_θ rather than p_s), w_g = 0.011 m [= 0.55/k_s (m)], and ω_r = -0.021 (= -1.046/k_s). The same calculations were conducted for all other c values.

(b) M_m and T_{mi} with movement w_f or R_L The evolution of the 'ultimate' M_m and T_{mi} with the frame movement, see Figure 15(a) and (b), is closely traced by Predictions I and II using α = 0.6 (= w_g/w_f, see G4). The response of M_m, T_{mi} and w_g for all tests with the sliding depth ratio R_L in Figure 16(a), (b) and (c), respectively, is also well replicated by β = 1.22 (with c = 0.82l_m, G1). Note the initial soil movement w_i (= 50 mm) and sliding depth ratio R_i (= 0.05–0.15) are considered in the comparison with the measured M_m and T_m. In particular, the T_{m2} (stable layer) is well prognosticated despite the overestimation of T_{m1} (sliding layer) against the measured data [see Figure 16(b)]. This is also evident in the measured profiles, shown in Figure 17, for a typical test TS32-0 at a sliding depth l_m of 200 mm. The 3-layer predictions with 13/50/10, indeed compare more favourably with the measured data than the 2-layer model [with m/k_s(kPa)/p_b(kN/m)= 7/60/12.5].

(c) Stiffness $\bar{k}_\theta$ versus z_m The impact of rotational stiffness k_θ on the shear force T_{m3} (stable layer) was presented previously in Figure 12(a) and (b). This is explored further, as an example, for the pile TS32-0 [P = 0, see Figure 1(b)] at a normalised sliding ratio l_m/l of 0.1. The calculated results as provided in Table IV indicate that an increase in the normalised rotational stiffness $\bar{k}_\theta$ from 0 to 0.952 renders (1) shift of the depth z_m towards the pile tip; (2) reduction in the M_m at z_m to zero

(from 10.9 Nm); (3) raise in the ground-line bending moment M_m from zero to -22.0 Nm; and (4) subtle augment in the T_{m1} [= -(65.2–66.8) N] and the T_{m2}, and a reduction in the T_{m3} from 40.01 N to zero. The lower layer fades for $\bar{k}_\theta$ = 0.952 at l_m/l = 0.1, as the M_m progresses to the pile-cap level ($z_m \rightarrow l$, or $\rightarrow$ 0), and T_{m3} = 0. This is consistent with Figure 12 despite the difference in m of 10 and 13. As indicated in Figure 12(a), the critical $\bar{k}_\theta$ dwindles with increasing l_m/l, and it drops to, for instance, about 0.3 at l_m/l = 0.4.

The same pile test with a vertical load P of 294 N (TS32-294) was also simulated using the aforementioned parameters but for α = 0.9 [see G4] and m =18 (see Table III). The prediction agrees well with the measured profiles (not shown herein).

5.2.2 Capped Piles with Limited p_b (α = 0.25–0.3)

The 3-layer solutions were employed to simulate the capped 2-piles (US32-0) in-line [see Figure 1(c_1)] under a uniform loading block. The piles are characterised by $k_A = k_\theta \neq 0$, $k_B = 0$, and $H = 0$. The predictions I and II adopted m/k_s(kPa)/p_b(kN/m)/$\bar{k}_\theta$ (see Table III) of 13/35/2.45/0.1 (design-state), and 17.7/16/3.0/0.15 (Ultimate state), respectively. The limiting p_b for the translating piles was estimated as 2.5–3.0 kN/m (= αp_{ub}, α ≈ 0.25–0.3, and p_{ub} = 10 kN/m), prior to which the piles are dominated by elastic-interaction. The interaction factor p_m is estimated as 0.83 (Pile A) and 0.35 (Pile B) for s/d = 3, which are reduced to 0.7 and 0.32 (due to the loading distance of 0.7l).

(a) Design State The 3-layer prediction I for design state was made using m = 13, k_s = 35 kPa (= 50p_m, p_m = 0.7), and k_θ = 1.2 kNm/rad (= 0.1×35×0.7^3). The predicted maximum moments in the pile and at the ground-line are plotted in Figure 18(a) against the displacement w_g. For the loading depth l_m of 0.2m, it follows c = 0.186 m [= 0.93×0.2 m, β = 1.08], and p_s = 0.652 kN/m [using Equation (7)]. The predicted p(z), M(z) and T(z) profiles for the l_m were predicted and are plotted in Figure 18(b) through (d). All the predictions compare well with the measured response, respectively. Crucially, the limited mobilization of p_s renders the maximum moments M_m= 11.5 Nm, at which the M_o is taken as a constant of M_m, regardless of the large sand movement w_f [= ~150 mm]. This is due to the limited, pile-soil relative defection w_g of ~ 7 mm [see Figure 19(c_2)]

(b) Ultimate State The 'Prediction II' for ultimate state was conducted by taking m =17.7, k_s = 16 kPa (= 50p_m, p_m = 0.32 ≈ α = 0.3), p_b = 3 kN/m, and $\bar{k}_\theta$ = 0.15. The prediction also well captures the evolution of the M_{mi} (i.e. M_m and the ground-line moment M_o) with w_g, the ultimate p(z), M(z), and T(z) in Figure 18; the evolution of the M_{mi} and the T_{mi} with the frame movement [see Figure 19(a) and (b)], and the M_{mi} with head-displacement w_g [see Figure 19(d)]; and the on-pile force per unit length [see Figure 19(e)], respectively. The prediction II offers a better agreement with the

measured M_o and w_g curve, and a higher limit of M_m [see Figure 19(a)] than Prediction I, which should be capped as ~ 12.0 Nm as well.

(c) Pile B and k_θ 'Prediction III' was carried out for 17.7/8/1.7/0.11, to capture the response of the Pile B (at P = 0) [see Figure 19(d) and (e)]. The parameters are reduced by a factor of 0.5–0.7 against pile A for shadowing effect, and k_s = 8 kPa (= 16p_m, p_m = 0.5–0.7), p_b = 1.7 (= 2.5p_m, p_m = 0.7), and $\bar{k}_\theta$ (=$\bar{k}_A$ = 0.11). The predictions agree with the measured data in Figure 19(d) and (e), respectively. The head-rotation angle for Pile A was estimated as 0.0123 radians, for a rotation stiffness k_θ of 0.823 kNm (via $\bar{k}_\theta = \bar{k}_A$ = 0.15, and k_s = 16 kPa) at a predicted moment M_o of 10.14 kNm. The angle for Pile B was estimated as 0.0195 radians for k_θ = 0.302 kNm (via $\bar{k}_\theta = \bar{k}_A = 0.11$, and k_s = 8 kPa) at a predicted M_o of 5.88 kNm. Despite the rigid cap, Pile A and B may have different rotation angles due to the discrepancy in the pile-cap connections. A factor λ_d of 0.667 and 0.5 [see Figure 19(c_1) and (c_2)] well captures the impact of cap-rotation on the increasing displacement with depth measured in the tests under P = 0 and P =294 N/pile, respectively.

6 PILES SUBJECTED TO LARGE EMBANKMENT MOVEMENT

The 3-layer model incorporates impact of 'dragging' on the piles. With the input parameters tabulated in Table III, it well predicts the response of the pile groups (in Test 9, Test 11 and BS test conducted in centrifuge) adjacent to embankments [14, 39] overlying a thick-clay layer, or a clay-sand layer, respectively. The prediction is illustrated next through the BS test.

Bransby and Springman [14] conducted centrifuge tests (termed as BS test) on a pile group of two infinitely long rows. Each pile (with a Young modulus of 40 GPa, a Poisson's ratio of 0.33) was 1.27 m in diameter, and 19 m in length, and was embedded in a 6 m-thick clay layer (s_u = 42.5 kPa) overlying dense sand ($\phi = 35^o$). The piles were installed at a spacing of 6.67 m along the pile row and 5 m between the rows, and have a rigid pile-cap 9 m wide and 1 m thick. The clay surface (outside the pile cap) was subjected to a uniform surcharge (sand cushion) of 17 kPa. The shear modulus was 7.5 MPa at the clay-sand interface, and increased by 7.5 MPa/m downwards. An increasing uniform surcharge pressure q was applied to the top soil surface 1 m away from one edge of the pile cap. The q induced the pile group displacement w_g, and rotation angle shown in Figure 20(a) and (b), respectively; the on-pile lateral pressure p_s/d depicted in Figure 20(c); the shear force mobilised along the interface between the pile-cap and the subsoil presented in Figure 20(d); and the profiles of bending moment $M(z)$ and on-pile lateral pressure (under a surcharge q of 200 kPa) provided in Figure 21(a) and (b), respectively. A 3-dimensional FEM analysis was also conducted [14] and is included in the figures, respectively.

6.1 3-layer Model Predictions

The 3-layer prediction was made for the piles (l = 19.0 m, d = 1.27 m) in a sliding layer (l_m = 6.0 m) using m =13.6, k_s = 881 kPa, p_b = 610 kN/m (p_{ub} = 845 kN/m, and α = 0.72 as with an inverse triangular soil movement [27]), and k_θ = 848 MNm/radian. The parameters are determined as follows: (1) The p_{ub} is equal to $1.38\times11s_u\times1.27l_m$/c for $l_m/l < 0.5$ (see G2a), in which s_u = 42.5 kPa; (2) The k_s is equal to 51(1.27)(13.61/0.271)] kPa using Equation (9) with K_{p1} = 3.69 and K_{a2} = 0.271 (ϕ = 35^o); (3) The α (= p_b/p_{ub}) is taken as 0.72 for the clay layer. It is estimated as 0.4–1.0 [= 1.3×(0.33–0.8), assuming 30 per cent increase from translation (α = 0.33) to rotation (α = 0.8) of due to embankment surcharge, G4a]; and (4) The k_θ is equal to $0.15\times881\times19^3$ using $\bar{k}_\theta = \bar{k}_A = 0.15$ as per the current model piles.

The displacement w_g, rotation angle and on-pile pressure (p_s/d) were predicted for a surcharge pressure q of ~ 250 kPa, as are plotted in Figure 20(a), (b) and (c), respectively, using the stipulated shear force on the pile-cap in Figure 20(d). Ignoring this shear force would offer 5% lower moment, and 5% higher displacement and rotational angle than what presented herein. The profiles of the bending moment and the on-pile pressure at a loading depth c of 5.8 m (= $0.97l_m$) were predicted and are plotted in Figure 21(a) and (b), respectively, along with the measured data. The soaring bending moment at the sliding depth is owing to the cap shear force in the 3-layer model. The predictions (bold lines) generally concur with the measured data.

6.2 Justification of k_s value

The modulus k_s may alternatively be estimated as $2.44G_{s1}$ for l/d = 15 [9] using secant shear modulus G_{s1}. The G_{s1} in turn is calculated by $G_{s1} = G_i[1-0.985(SML)^{0.2}]$ [39] using the initial shear modulus G_i, and the average stress mobilization level (SML) for the embankment. The SML [= $(0.5/\alpha)c/l_m$] at c/l_m = 0.97 is estimated 0.97 (α = 0.5) and 0.674 (α = 0.72) for an 'arc' profile and a linear profile of soil movement, respectively [27]. The modulus G_i is equal to 5.17 MPa for a Young's modulus of 15 MPa [14] (Case I), or 7.5 MPa (at the clay and sand interface, Case II). The associated modulus k_s is estimated as follows.

- Case I (G_i = 5.17 MPa): At α = 0.5, it follows G_{s1} = 108.5 kPa = $5{,}170[1-0.985(0.97)^{0.2}]$ and k_s = 264 kPa; and k_s = 1,134 kPa (with G_{s1} = 464.7 kPa) at α = 0.72. The average k_s for α = 0.5–0.72 is 699 kPa.
- Case II (G_i = 7.5 MPa): The k_s was estimated as 384 kPa (α = 0.5) – 1,644 kPa (α = 0.72), with an average of 1,014 kPa.

The average k_s of 699 kPa (Case I) −1,014 kPa (Case II) is 856.7 kPa (3% less than 881 kPa), which would lead to a similar prediction to what presented here.

The 2-layer model was used to predict the pile response using the same parameters (but for m = 8.17), and is presented in the figures. It yields a slightly smaller displacement, rotation, but a higher lateral on-pile pressure. The moment conforms with measured data (without shear force). The shear force profile is of similar shape to the FEM prediction. Importantly, Figure 21(b) indicates that introducing the transition layer allows excellent capture of the lateral on-pile pressure, which is not realised by the 3-D FEM analysis. The predictions were repeated for Tests 9 and 11, which are quite satisfactory using the five parameters p_b, k_s, m, k_θ, and α in Table III. Conversely, the parameters may be deduced using the measured pile response.

7 CONCLUSIONS

This paper develops a 3-layer model and elastic solutions to capture nonlinear response of rigid, passive piles in sliding soil. Elastic solutions are obtained for an equivalent force per unit length p_s of the soil movement. They are repeated for a series of linearly increasing p_s (with depth) to yield the nonlinear response. The parameters underpinning the model are determined against pertinent numerical solutions and model tests on passive free-head, and capped piles. The solutions are presented in non-dimensional charts, and elaborated through three examples. The study reveals the following:

- On-pile pressure in rotationally restrained, sliding layer reduces by a factor α, which resembles the p-multiplier for a laterally loaded, capped pile, but for its increase with vertical loading (embankment surcharge), and stiffness of underlying stiff layer: α = 0.25 and 0.6 for a shallow translating and rotating piles, respectively; α = 0.3–0.5 and 0.8–1.3 for a slide overlying a stiff layer concerning a uniform and a linearly increasing pressure, respectively; and α = 0.5–0.72 for moving clay under embankment loading.
- Ultimate state is well defined using the ratio of passive earth pressure coefficient over that of active earth pressure: $m = (0.7–1.0)K_{p1}/K_{a2}$ during a large, overlying soil movement; or $m = 2.1K_{p1}/K_{a2}$ for a sliding sand over soft rock. The subgrade modulus k_{s2} of underlying sand for a large soil movement (typically > 0.5 m) may be scaled from model tests using Equation (9).
- The normalised rotational stiffness is equal to 0.1–0.15 for the model 2-piles and embankment piles, which reduces the pile displacement with depth by a magnitude of $(0.5–0.667)zM_m/k_\theta$.

The 3-layer model well predicts nonlinear response of the capped piles subjected to soil movement, which may be used for pertinent design. The factor α and normalised rotational stiffness $\bar{k}_\theta$ are

critical to the prediction, which are discussed at length in subsequent publications using model tests.

8 ACKNOWLEDGMENTS

The author is grateful for the anonymous reviewer's comments, which render improvement of this article.

REFERENCES

1. Guo, W.D. *A simplified approach for piles due to soil movement*. in *Proc. 12th Panamerican conference on soil mechanics and geotechnical engineering*. 2003; Cambridge, Massachusettes, USA: Verlag Gluckauf GMBH. Essen (Germany).
2. Guo, W.D., *p_u based solutions for slope stabilising piles.* International Journal of Geomechanics, 2013; **13**(3): 292-310.
3. Fukuoka, M. *The effect of horizontal loads on piles due to landslides*. in *Proceedings 9th International Conference on Soil Mechanics and Foundation Engineering, Speciality session 10*. 1977; Tokyo.
4. Cai, F. and K. Ugai, *Response of flexible piles under laterally linear movement of the sliding layer in landslides.* Canadian Geotechnical Journal, 2003; **40**(1): 46-53.
5. Chmoulian, A., *Briefing: Analysis of piled stabilization of landslides.* Proceedings of the Institution of Civil Engineers, Geotechnical Engineering, 2004; **157**(2): 55-56.
6. De Beer, E. and R. Carpentier, *Discussion on 'Methods to estimate lateral force acting on stabilising piles' By Ito, T., and Matsui, T. (1975).* Soil and Foundations, 1977; **17**(1): 68-82.
7. Ito, T. and T. Matsui, *Methods to estimate lateral force acting on stabilizing piles.* Soils and Foundations, 1975; **15**(4): 43-59.
8. Viggiani, C. *Ultimate lateral load on piles used to stabilise landslide*. in *Proc. 10th Int. Conf. Soil Mech. and Found. Engrg*. 1981; Stockholm, Sweden.
9. Guo, W.D., *Theory and practice of pile foundations*. 2012, Boca Raton, London, New York: CRC press.
10. Guo, W.D. and E.H. Ghee. *A preliminary investigation into the effect of axial load on piles subjected to lateral soil movement*. in *Proceedings of 1st International Symposium on Frontiers in Offshore Geotechnics*. 2005; Perth, Australia: Taylor & Francis.
11. Guo, W.D., *Elastic models for nonlinear response of rigid passive piles.* International Journal for Numerical and Analytical Methods in Geomechanics, 2014; **38**(18): 1969-1989.
12. Guo, W.D., *Nonlinear response of lateral piles with compatible cap stiffness and p-multiplier.* Journal of Engineering Mechanics, 2015; **141**(9): 06015002.
13. Brown, D.A., C. Morrison, and L.C. Reese, *Lateral load behaviour of pile group in sand.* Journal of Geotechnical and Geoenvironmental Engineering Division, ASCE, 1998; **114**(11): 1261-1276.
14. Bransby, M.F. and S.M. Springman, *3-D finite element modelling of pile groups adjacent to surcharge loads.* Computers and Geotechnics, 1996; **19**(4): 301-324.
15. Chow, Y.K., *Analysis of piles used for slope stabilization.* International Journal for Numerical and Analytical Methods in Geomechanics, 1996; **20**(9): 635-646.
16. Poulos, H.G., *Design of reinforcing piles to increase slope stability.* Canadian Geotechnical Journal, 1995; **32**(5): 808-818.
17. Brandenberg, S.J., M. Zhao, R.W. Boulanger, and D.W. Wilson, *p-y plasticity model for nonlinear dynamic analysis of piles in liquefiable soil.* Journal of Geotechnical and Geoenvironmental Engineering, ASCE, 2005; **139**(8): 1262-1274.

18. Poulos, H.G., L.T. Chen, and T.S. Hull, *Model tests on single piles subjected to lateral soil movement.* Soils and Foundations, 1995; **35**(4): 85-92.
19. Randolph, M.F. and G.T. Houlsby, *The limiting pressure on a circular pile loaded laterally in cohesive soil.* Geotechnique, 1984; **34**(4): 613-623.
20. Chen, L.T., H.G. Poulos, C.F. Leung, Y.K. Chow, and R.F. Shen, *Discussion of "Behavior of pile subject to excavation-induced soil movement.".* Journal of Geotechnical and Geoenvironmental Engineering, ASCE, 2002; **128**(3): 279-281.
21. Frank, R. and P. Pouget, *Experimental pile subjected to long duration thrusts owing to a moving slope.* Geotechnique, 2008; **58**(8): 645-658.
22. Smethurst, J.A. and W. Powrie, *Monitoring and analysis of the bending behaviour of discrete piles used to stabilise a railway embankment.* Geotechnique, 2007; **57**(8): 663-677.
23. Franke, K.W. and K.M. Rollins, *Simplified hybrid p-y spring model for liquefied soils.* Journal of Geotechnical and Geoenvironmental Engineering, ASCE, 2013; **139**(4): 564-576.
24. Muraro, S., A. Madaschi, and A. Gajo, *On the reliability of 3D numerical analyses on passive piles used for slope stabilisation in frictional soils.* Geotechnique, 2014; **64**(6): 486-492.
25. Guo, W.D., *On limiting force profile, slip depth and lateral pile response.* Computers and Geotechnics, 2006; **33**(1): 47-67.
26. Guo, W.D., *Laterally loaded rigid piles in cohesionless soil.* Canadian Geotechnical Journal, 2008; **45**(5): 676-697.
27. Guo, W.D., *Nonlinear response of laterally loaded rigid piles in sliding soil* Canadian Geotechnical Journal, 2015; **52**(7): 903-925.
28. Dobry, R., T. Abdoun, T.D. O'Rourke, and S.H. Goh, *Single piles in lateral spreads: field bending moment evaluation.* Journal of Geotechnical and Geoenvironmental Engineering, ASCE, 2003; **129**(10): 879-889.
29. He, L., A. Elgamal, T. Abdoun, A. Abe, R. Dobry, M. Hamada, J. Menses, M. Sato, T. Shantz, and K. Tokimatsu, *Liquefaction-induced lateral load on pile in a medium Dr sand layer.* Journal of Earthquake Engineering, 2009; **13**: 916-938.
30. Mokwa, R.L. and J.M. Duncan, *Discussion on 'Centrifuge model study of laterally loaded pile groups in clay' by T. IIyas, C. F. Leung, Y. K. Chow and S. S. Budi.* Journal of Geotechnical and Geoenvironmental Engineering Division, ASCE, 2005; **131**(10): 1305-1307.
31. Juirnarongrit, T. and S.A. Ashford, *Soil-pile responese to blast-induced lateral spreading II: Analysis and assessment of the p-y method.* Journal of Geotechnical and Geoenvironmental Engineering Division, ASCE, 2006; **132**(2): 163-172.
32. Abdoun, T., R. Dobry, T.D. O'Rourke, and S.H. Goh, *Pile response to lateral spreads: Centrifuge modeling.* Journal of Geotechnical and Geoenvironmental Engineering, ASCE, 2003; **129**(10): 869-878.
33. Brandenberg, S.J., R.W. Boulanger, and B.L. Kutter, *Discussion of "Single piles in lateral spreads: field bending moment evaluation" by R. Dobry, T. Abdoun, T. D. O'Rourke, and S. H. Goh.* Journal of Geotechnical and Geoenvironmental Engineering, ASCE, 2005; **131**(4): 529-534.
34. Poulos, H.G. and E.H. Davis, *Pile foundation analysis and design*. 1980, New York: John Wiley & Sons.
35. Yang, Z. and B. Jeremic, *Numerical analysis of pile behaviour under lateral load in layered elastic-plastic soils.* Int. J. Numer. and Anal. Meth. in Geomech., 2002; **26**(14): 1385-1406.
36. Barton, Y.O., *Laterally loaded model piles in sand: Centrifuge tests and finite element analysis.* 1982; University of Cambridge.
37. JRA, *Specification for highway bridges*, in *Japan Road Association, Prepared by Public Works Research Institute (PWRI) and Civil Engineering Research Laboratory (CRL)*. 2002: Japan.

38. Guo, W.D. and H.Y. Qin, *Thrust and bending moment of rigid piles subjected to moving soil.* Can. Geotech. J., 2010; **47**(2): 180-196.
39. Stewart, D.P., R.J. Jewell, and M.F. Randolph, *Design of piled bridge abutment on soft clay for loading from lateral soil movements.* Geotechnique, 1994; **44**(2): 277-296.
40. Ishihara, K. and M. Cubrinovski. *Soil-pile interaction in liquefied deposits undergoing lateral spreading*. in *Proc. XI Danube-European Conference, May*. 1998; Croatia.
41. Ishihara, K. and M. Cubrinovski. *Case studies of pile foundations undergoing lateral spreading in liquefied deposits*. in *Proc. Fifth nternational Conference on Case Histories in Geotechnical Engineering, April 13-17*. 2004; New York, NY.
42. Guo, W.D. and E.H. Ghee. *Response of axially loaded pile groups subjected to lateral soil movement - An expremental investigation*. in *Proceedings of 6th International Conference on Tall Buildings (ICTB-VI)*. 2005; Hong Kong, China: World Scientific Publishing Co. Pte. Ltd.
43. Kourkoulis, R., F. Gelagoti, I. Anastasopoulos, and G. Gazetas, *Slope stabilizing piles and pile-groups: parametric study and design insights.* Journal of Geotechnical and Geoenvironmental Engineering, ASCE, 2011; **137**(7): 663-677.
44. Leung, C.F., Y.K. Chow, and R.F. Shen, *Behaviour of pile subject to excavation-induced soil movement.* Journal of Geotechnical and Geoenvironmental Engineering, American Society of Civil Engineers, 2000; **126**(11): 947-954.

NOTATION

The following symbols are used in the paper:

c = loading depth, or cohesion;

d = diameter of an equivalent solid cylinder pile;

G_i, G_{si}, G_{av} = initial shear modulus, shear modulus over the sliding depth (i =1) and stable layer (i = 2), and an average soil shear modulus over the pile embedment;

H = shear force just about a liquefied layer, induced by a upper, non-liquefied layer;

K_{a2} = coefficient of active earth pressure of stable layer;

k_A, k_B, k_θ = rotational stiffness of a pile-cap (or a non-liquefied layer), and a stable layer, underlying a liquefied layer, and total rotational stiffness of a pile, respectively;

k_i = coefficient for limiting resistance for upper layer (i = 1) and lower layer (i = 2);

K_{p1} = coefficient of passive earth pressure of sliding layer;

k_s = modulus of subgrade reaction of the sliding layer;

l, l_m = embedded pile length, and thickness of a upper moving soil layer, respectively;

LIFPULD = **l**inearly **i**ncreasing **f**orce **p**er **u**nit **l**ength with **d**epth;

M_A, M_B = constraint moment at the top and bottom of a liquefied layer, respectively.

$M_i(z)$ = bending moment at depth z;

M_m (M_o) = maximum bending moment within a pile (or at the mudline level);

m = ratio of the subgrade modulus of the stable layer k_{s2} over that of the upper sliding layer k_s;

P = vertical load on passive piles during model tests;

p_s = limiting force per unit length in sliding layer due to soil movement ($\geq w_s^* = p_s/k_s$);

$p(z)$, $p_i(z)$ = net on-pile force per unit length at a depth z; on-pile force per unit length at a depth z calculated for sliding (i =1), transition (2), and stable (3) layer, respectively using the elastic solutions;

p_u = limiting force per unit length along a laterally loaded, free-head pile;

p_{ub} (p_b) = limiting force per unit length at the base of a free-head pile during passive loading, and p_b = αp_{ub} for rotationally restrained piles;

p_{ui} = limiting force per unit length p_u for a pile in sliding (i =1), and stable (2) layer, respectively, which are used for estimating the modulus k_s;

q = $p_s/(\alpha d)$, surcharge pressure of an embankment loading;

s_u = undrained shear strength of soil;

T_m = maximum shear force induced in a passive pile;

$T(z)$, $T_i(z)$ = shear force at depth z;

w_f, w_s = frame movement in model pile tests, w_s (= $w_s^* = p_s/k_s$), effective soil movement;

w_g = pile-displacement at ground level;

$\overline{w}_g$ = $w_g k_s/p_s$, normalised pile-displacement at ground level;

$w(z)$,w'(z) = displacement and rotation at depth z;

z, $\overline{z}$ = depth and the normalised depth z/l, respectively;

$z_{m,}$ z_{mi} = depth of maximum bending moment (i = 1, 2);

α = a factor for soil movement profile, or ratio of on-pile pressure over the embankment pressure;

β = c/l_m, effective depth of sliding layer c over intended sliding depth l_m;

γ' = effective unit weight of clay or sand;

λ = modification ratio in estimating k_s;

λ_d = 0.5–0.667, distribution factor for displacement due to cap-restraining stiffness;

ω_r = rotation angle of pile at ground-level

$\overline{\omega}_r$ = $w'(z)k_s l/p_s$, normalised rotation angle;

ϕ = angle of internal friction;

ψ = angle of dilatancy.

Bar '-' for normalised parameters and variables. Depths c, z, l_m are all normalised by pile embedment length l.

Table I 3- layer solutions for passive piles

Depth z	Sliding layer with k_s, $z \le l_m$, $p_1(z) = (\overline{\omega}_r \bar{z} + \overline{w}_g) p_s$, $p(z) = p_1(z) - p_s$
Shear force $T(z)$	$\dfrac{T_1(z)}{p_s l} = 0.5\overline{\omega}_r \bar{z}^2 + \overline{w}_g \bar{z} - \bar{z} - \overline{H}$
Moment $M(z)$	$\dfrac{M_1(z)}{p_s l^2} = \dfrac{1}{6}\overline{\omega}_r \bar{z}^3 + \dfrac{1}{2}(\overline{w}_g - 1)\bar{z}^2 - \overline{H}\bar{z} + \bar{k}_A \overline{\omega}_r$ $\quad \bar{k}_A = k_A/(k_s l^3)$
Depth	k_s *transition layer,* $l_m \le z \le z_m$
$p(z)$	$p(z) = p_2(z) = (\overline{\omega}_r \bar{z} + \overline{w}_g)[(m-1)\dfrac{\bar{z} - \bar{l}_m}{\bar{z}_m - \bar{l}_m} + 1] p_s$
Shear force $T(z)$	$\dfrac{T_2(z)}{p_s l} = \dfrac{1}{6(\bar{l}_m - \bar{z}_m)}\{(1-m)[3\overline{w}_g(\bar{z}^2 + \bar{l}_m^2) + \overline{\omega}_r(2\bar{z}^3 + \bar{l}_m^3)]$ $- 3(\bar{z}_m - m\bar{l}_m)(2\overline{w}_g + \bar{z}\overline{\omega}_r)\bar{z}\} - \overline{H} - \bar{l}_m$
Bending moment $M(z)$	$\dfrac{M_2(z)}{p_s l^2} = \dfrac{1}{12(\bar{l}_m - \bar{z}_m)}\{(1-m)[2\overline{w}_g(\bar{z}^3 + 3\bar{l}_m^2\bar{z} - \bar{l}_m^3) + \overline{\omega}_r(\bar{z}^4 + 2\bar{l}_m^3\bar{z} - \bar{l}_m^4)]$ $- 2(\bar{z}_m - m\bar{l}_m)(3\overline{w}_g + \overline{\omega}_r\bar{z})\bar{z}^2\} - \overline{H}\bar{z} - (\bar{z} - 0.5\bar{l}_m)\bar{l}_m + \bar{k}_A\overline{\omega}_r$
Depth z	*Layer with* mk_s, $z_m \le z \le l$, $p(z) = p_3(z) = (\overline{\omega}_r \bar{z} + \overline{w}_g) m p_s$
Shear force $T(z)$	$\dfrac{T_3(z)}{p_s l} = [\dfrac{1-m}{2}(\bar{l}_m + \bar{z}_m) + m\bar{z}]\overline{w}_g + [\dfrac{1-m}{6}(\bar{l}_m^2 + \bar{l}_m\bar{z}_m + \bar{z}_m^2)\bar{l}_m + \dfrac{m}{2}\bar{z}^2]\overline{\omega}_r - \bar{l}_m - \overline{H}$
Bending moment $M(z)$	$\dfrac{M_3(z)}{p_s l^2} = \dfrac{1-m}{12}\{2(\overline{\omega}_r\bar{z} - \overline{w}_g)(\bar{z}_m^2 + \bar{l}_m\bar{z}_m + \bar{l}_m^2) + [6\overline{w}_g\bar{z} - \overline{\omega}_r(\bar{l}_m^2 + \bar{z}_m^2)](\bar{l}_m + \bar{z}_m)\}$ $+ \dfrac{m}{6}\bar{z}^2(3\overline{w}_g + \overline{\omega}_r\bar{z}) - \overline{H}\bar{z} - (\bar{z} - 0.5\bar{l}_m)\bar{l}_m + \bar{k}_A\overline{\omega}_r$
$k_\theta = 0$	$\bar{z}_m = z_m / l = 0.5(-\overline{B} - \sqrt{\overline{B}^2 - 4\overline{C}})$
Note	$w(z) = (\overline{\omega}_r \bar{z} + \overline{w}_g) p_s / k_s$ $\dfrac{w_g k_s}{p_s} = \overline{w}_g = \dfrac{-6(1+\bar{z}_m)(\overline{H} + \bar{l}_m)}{(m-1)(-2\bar{l}_m^2 + \bar{z}_m\bar{l}_m + 3\bar{l}_m + \bar{z}_m^2) - 3(1+m)\bar{z}_m}$ $\dfrac{\omega_r k_s l}{p_s} = \overline{\omega}_r = \dfrac{12(\overline{H} + \bar{l}_m)}{(m-1)(-2\bar{l}_m^2 + \bar{z}_m\bar{l}_m + 3\bar{l}_m + \bar{z}_m^2) - 3(1+m)\bar{z}_m}$ $\overline{B} = \dfrac{3 + [3(1+m) + \bar{l}_m(1-m)]\overline{C}_1}{(1-m)\overline{C}_1}$ $\overline{C} = \dfrac{m - (m-1)\bar{l}_m[3(\overline{C}_1 + 1) + \bar{l}_m(\bar{l}_m - 2\overline{C}_1 - 3)]}{(1-m)\overline{C}_1}$ $\overline{C}_1 = \dfrac{\bar{k}_\theta\overline{\omega}_r + \overline{H} + \bar{l}_m(1 - 0.5\bar{l}_m)}{-(\overline{H} + \bar{l}_m)}$ $\quad k_\theta = k_A + k_B$ $\quad \bar{l}_m = l_m / l$ $\quad \overline{H} = H/(p_s l)$ $\bar{k}_\theta = k_\theta/(k_s l^3)$

Table II Determination of m and subgrade modulus k_s

Case	l_2 [a] /l_m	Sliding/ stable layer	Angle ϕ	K_{p1}/K_{a2}	p_{u2}/p_{u1}	m	l_{2c}/l_m	λ	k_s (kPa)
I	0-1.5	Sand/sand	23°/23°	5.21		5.21	1.0	1.0	
	0-1.5			5.21		10.42	1.0	1.0	
	0-1.5			5.21		15.63	1.0	1.0	
II	0.7	Loose sand/ loose sand	28°/28°	7.62	1.0	5.37	1.0	3.0	1,404
	1.0		28°/28°	7.62	1.0	7.62	1.0	2.5	1,170
	1.2			7.62	1.0	7.62	1.2	2.0	1,348
	1.5			7.62	1.0	7.62	1.3	1.5	1,187
III	0.7	Loose sand/ dense sand	28°/38°	11.64	1.6	8.15	1.0	3.0	2,247
	1.0			11.64	1.6	11.64	1.0	2.0	1,498
	1.2			11.64	1.6	11.64	1.2	1.5	1,618
	1.5			11.64	1.6	11.64	1.2	1.0	2,427
IV	0.7	Loose sand/ soft rock	28°/45°	16.14	3.0	33.9	1.0	1.5	2,107
	1.2			16.14	3.0	33.9	1.0	1.0	1,404
	1.5			16.14	3.0	33.9	1.0	1.0	1,404

[a] Thickness of the stable layer.

Table III Parameters for 3-layer model predictions of typical piles

Cases	c/l_m [a]	m/p_{ub} (kN/m) [a]	k_s (kPa) /d (cm) [a]	$\bar{k}_\theta$ [a]	α	ϕ	Reference
TS32-294	0.82	18/12.5	50/3.2	0	0.9	38	[38]
TS32-0	0.82	13/12.5	50/3.2	0	0.6	38	
US32-0	0.93	13-17.7/10	38.5/3.2	0.1	0.25-0.3	38	[42]
Test 9	0.77	17.7/46.4	20/43	0.007	0.5	38	[39]
Test 11	0.83	17.7/85	20/43	0.1	0.72	38	
BS test	0.97	13.6/610	881/127	0.15	0.72	35	[14]

Note [a] in the second through to fourth columns, the values of c/l_m, m, p_{ub}, k_s, $\bar{k}_\theta$ and α along with l, l_m, d are all input values. [b] The reduced value of p_s is owing to limited depth of rotation, but largely translation of the pile.

Table IV Impact of k_θ on d_{32} pile in sliding soil at $l_m/l = 0.1$ [a]

$\bar{k}_\theta$	$\bar{z}_m / \bar{z}_{mt3}$	$\bar{w}_g$	$\bar{\omega}_r$	w_g(mm)	M_m (Nm)	ω_r (rad)	T_{mi} (N) [c]
0	0.417/0.709	0.073	-0.148	1.8	10.9/0 [b]	0.0037	-65.22/-65.81/40.01
0.2	0.513/0.756	0.063	-0.119	1.26	5.11/-8.16	0.0024	-65.88/-66.55/22.49
0.4	0.618/0.809	0.056	-0.099	1.12	2.06/-13.62	0.0020	-66.31/-67.07/11.55
0.6	0.736/0.868	0.052	-0.085	1.03	0.58/-17.50	0.0017	-66.59/-67.46/4.73
0.8	0.874/0.937	0.049	-0.074	0.97	0.06/-20.34	0.0015	-66.78/-67.78/0.94
0.952	1.0/1.02	0.047	-0.067	0.94	0/-22.00	0.0014	-66.86/-68.01/0.0

[a] m =13, H = 0; [b] $k_A = k_\theta$, value before and after sign '/' for M_m locates at depth z_m and cap-level, respectively. [c] The first, the middle and the last values are for the sliding, transition, and stable layer, respectively.

Figure Captions

Figure 1 Rigid piles tested under one of the indicated soil movement profiles. (a) Elevation view of the shear apparatus, (b_1) Inverse triangular movement, (c_1) Uniform movement, (b_2) and (c_2) theoretical mode for the test in (b_1) and (c_1).

Figure 2 Models for rigid, passive pile: (a) Non-linear model, (b) p_b and p_s, (c) Pile - soil system, (d) p_s applied & $p(z)$ induced, (e) Model with k_A & k_B, (f) p_s applied for nonlinear response

Figure 3 (a) $T_m/(p_s l_m)$ versus normalized loading depth, (b) $M_m/(p_s l l_m)$ versus normalized shear force $T_m/(p_s l_m)$, and typical test data (uniform p_s)

Figure 4 $T_m/(p_s l_m)$ versus normalized layer thickness ratio: (a) 2-layer model, (b) *3*-layer model (linearly increasing p_s)

Figure 5 Predicted versus measured evolution of total thrust on piles in loose sand overlying loose sand: (a) pile-head displacement w_g, (b) maximum bending moment.

Figure 6 Predicted versus measured evolution of total thrust on piles in loose sand overlying dense sand: (a) pile-head displacement w_g, (b) maximum bending moment.

Figure 7 Predicted versus measured evolution of total thrust on piles in loose sand overlying soft rock: (a) pile-head displacement w_g, (b) maximum bending moment.

Figure 8 Normalized uniform soil movement w_g (constant k_s) with loading depth owing to (a) normalized rotational stiffness (m = 10), (b) normalized rotational stiffness (m = 1), (c) modulus ratio m ($\bar{k}_\theta = 0.1$)

Figure 9 Normalized pile rotational displacement (constant k_s) versus normalized pile-head displacement owing to (a) normalized rotational stiffness (m = 10 or 1), (b) modulus ratio m ($\bar{k}_\theta = 0.1$)

Figure 10 Normalized bending moment for base restrained piles with normalized soil movement w_s (constant k_s, and $k_B = k_\theta$) at z_m and l_m: (a) $\bar{k}_\theta$ = 0-3 and m = 1, (b) $\bar{k}_\theta = 0.1$ and m =1-21

Figure 11 Normalized thrust at sliding depth owing to (a) normalized rotational stiffness (m = 10), (b) the modulus ratio m ($\bar{k}_\theta = 0.1/0.05$)

Figure 12 Normalized thrust T_m owing to (a) normalized rotational stiffness (m = 10), (b) the modulus ratio m ($\bar{k}_\theta = 0.1$).

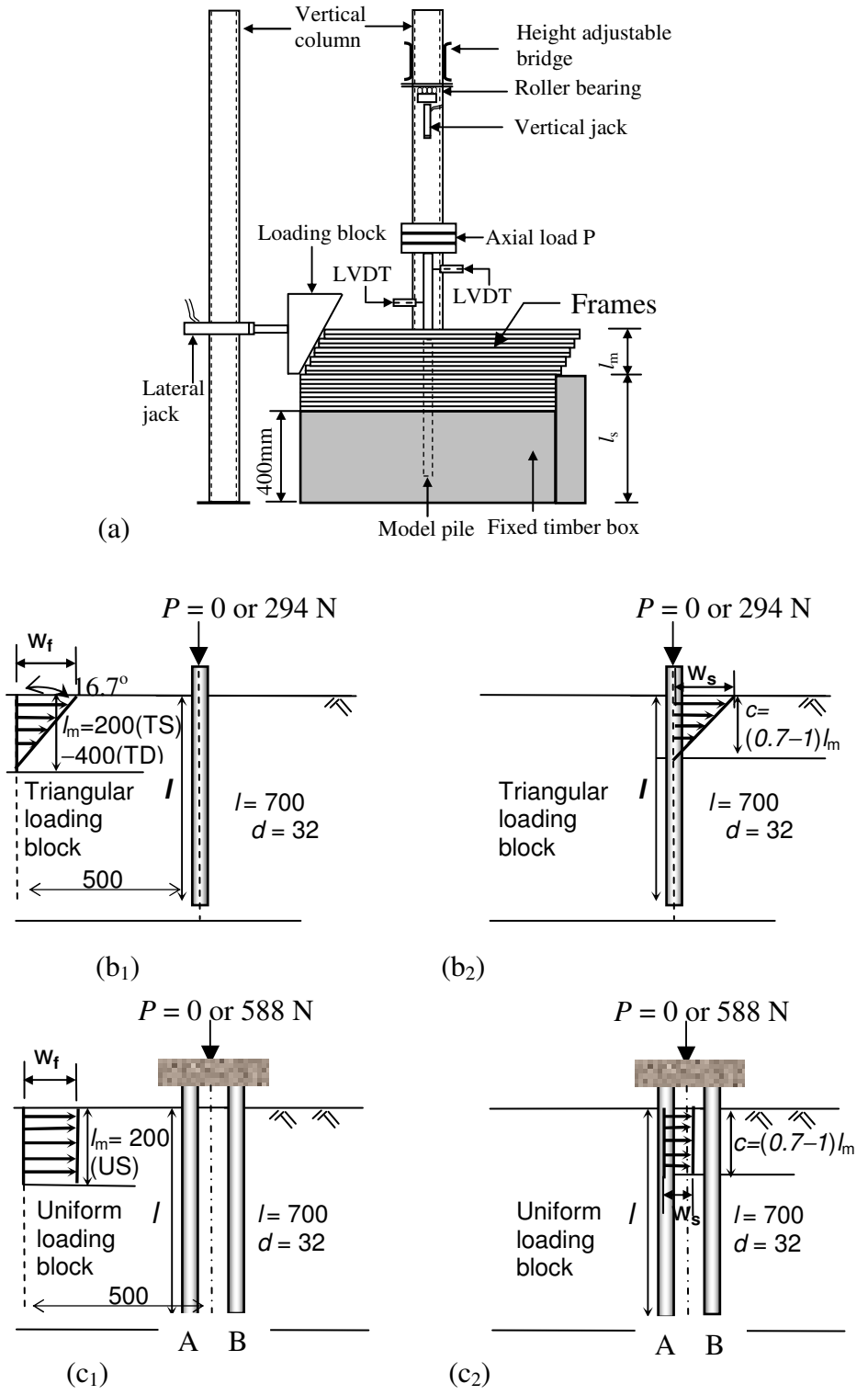

Figure 1 Rigid piles tested under one of the indicated soil movement profiles. (a) Elevation view of the shear apparatus, (b_1) Inverse triangular movement, (c_1) Uniform movement, (b_2) and (c_2) theoretical mode for the test in (b_1) and (c_1).

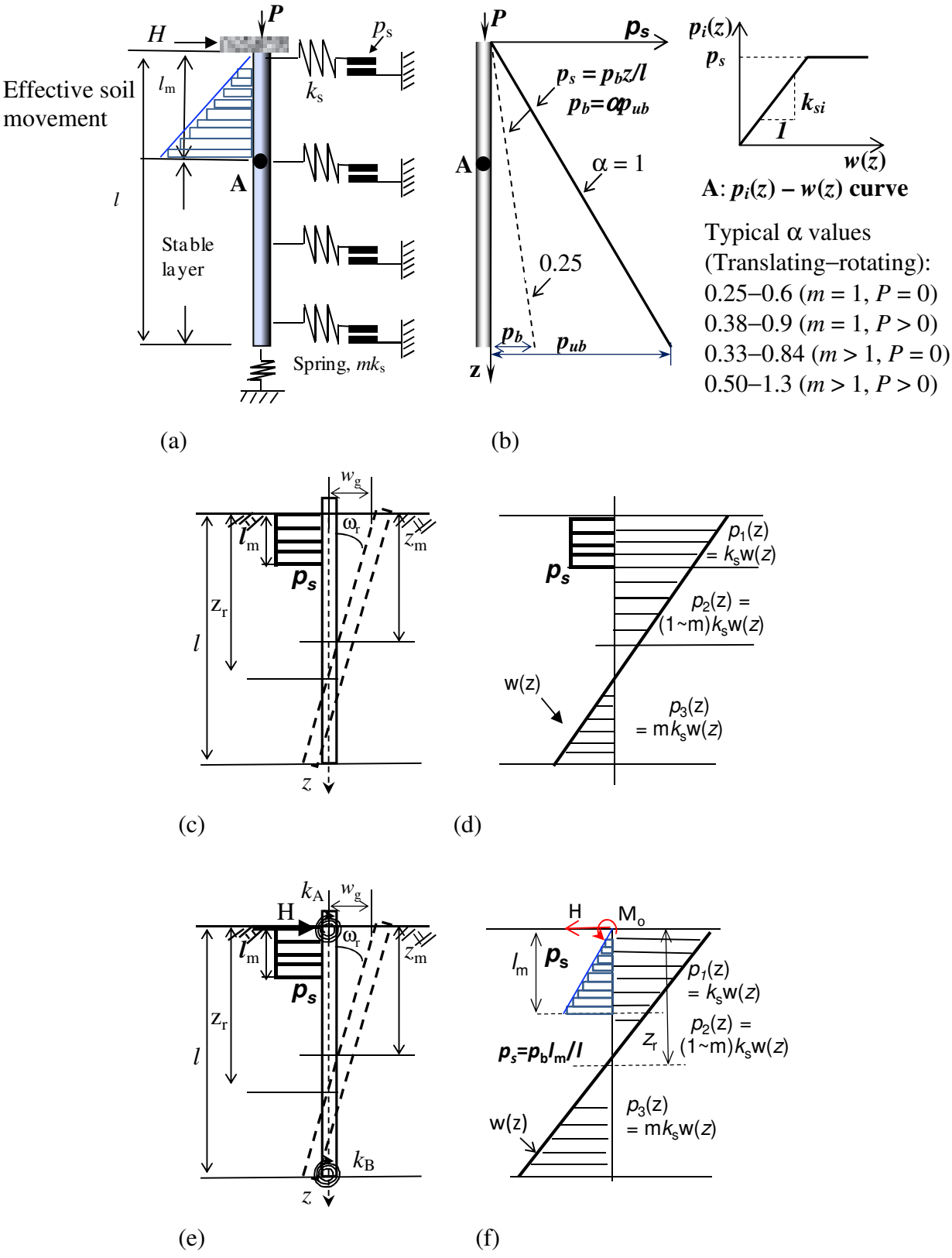

Figure 2 Models for rigid, passive pile: (a) Non-linear model, (b) p_b and p_s, (c) Pile - soil system, (d) p_s applied & $p(z)$ induced, (e) Model with k_A & k_B, (f) p_s applied for nonlinear response

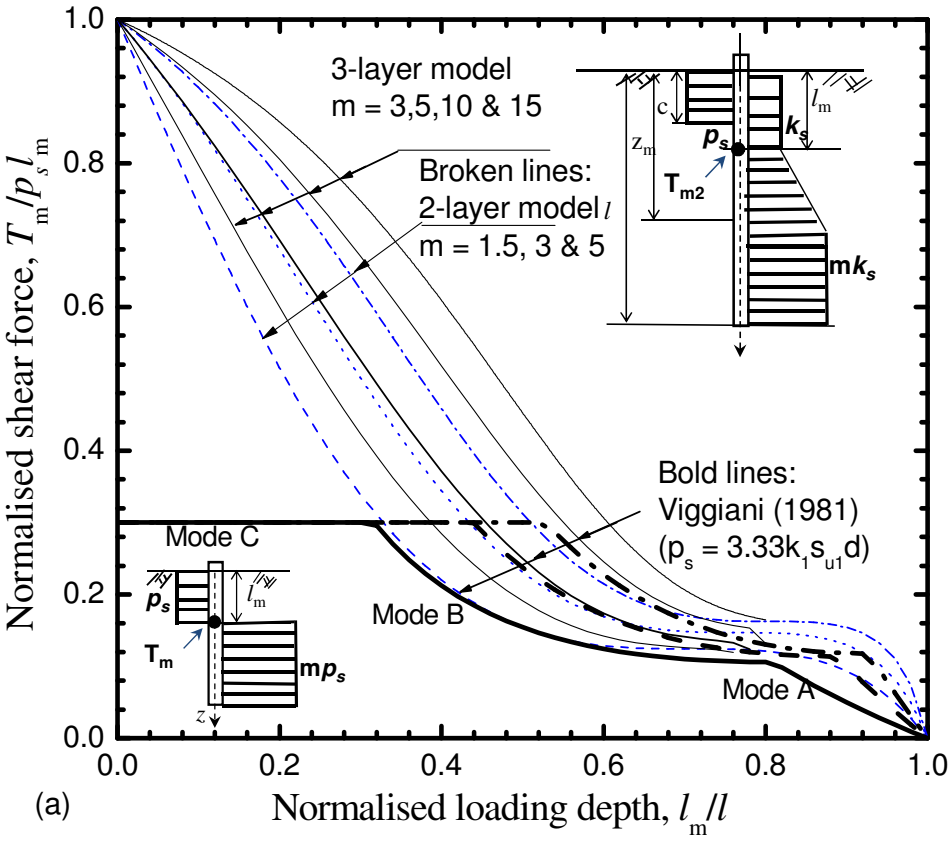

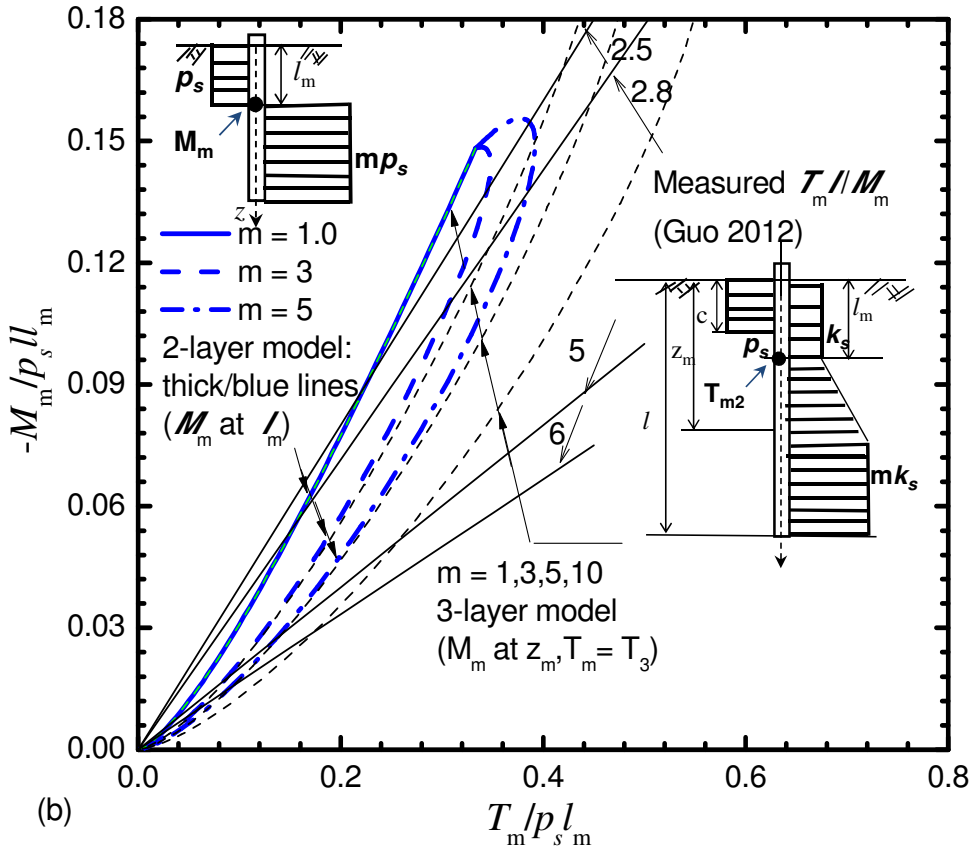

Figure 3 (a) $T_m/(p_s l_m)$ versus normalized loading depth (b) $M_m/(p_s l l_m)$ versus normalized shear force $T_m/(p_s l_m)$, and typical test data (uniform p_s)

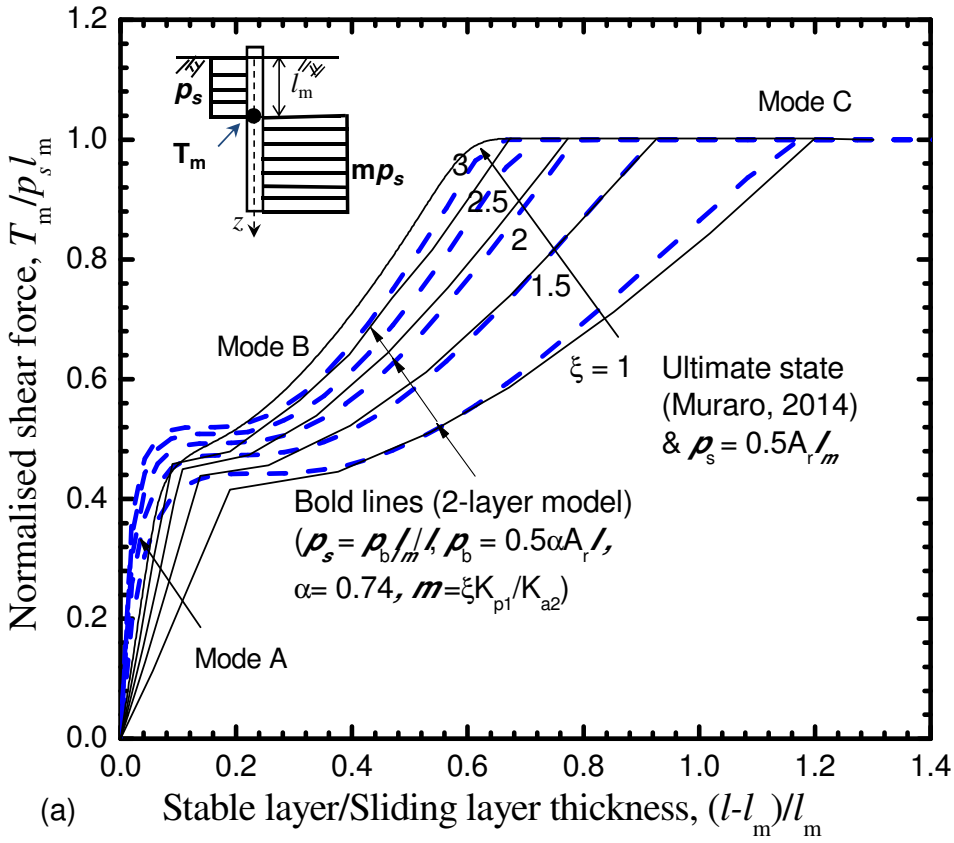

Figure 4 $T_m/(p_s l_m)$ versus normalized layer thickness ratio: (a) 2-layer model, (b) *3*-layer model for a linearly increasing p_u

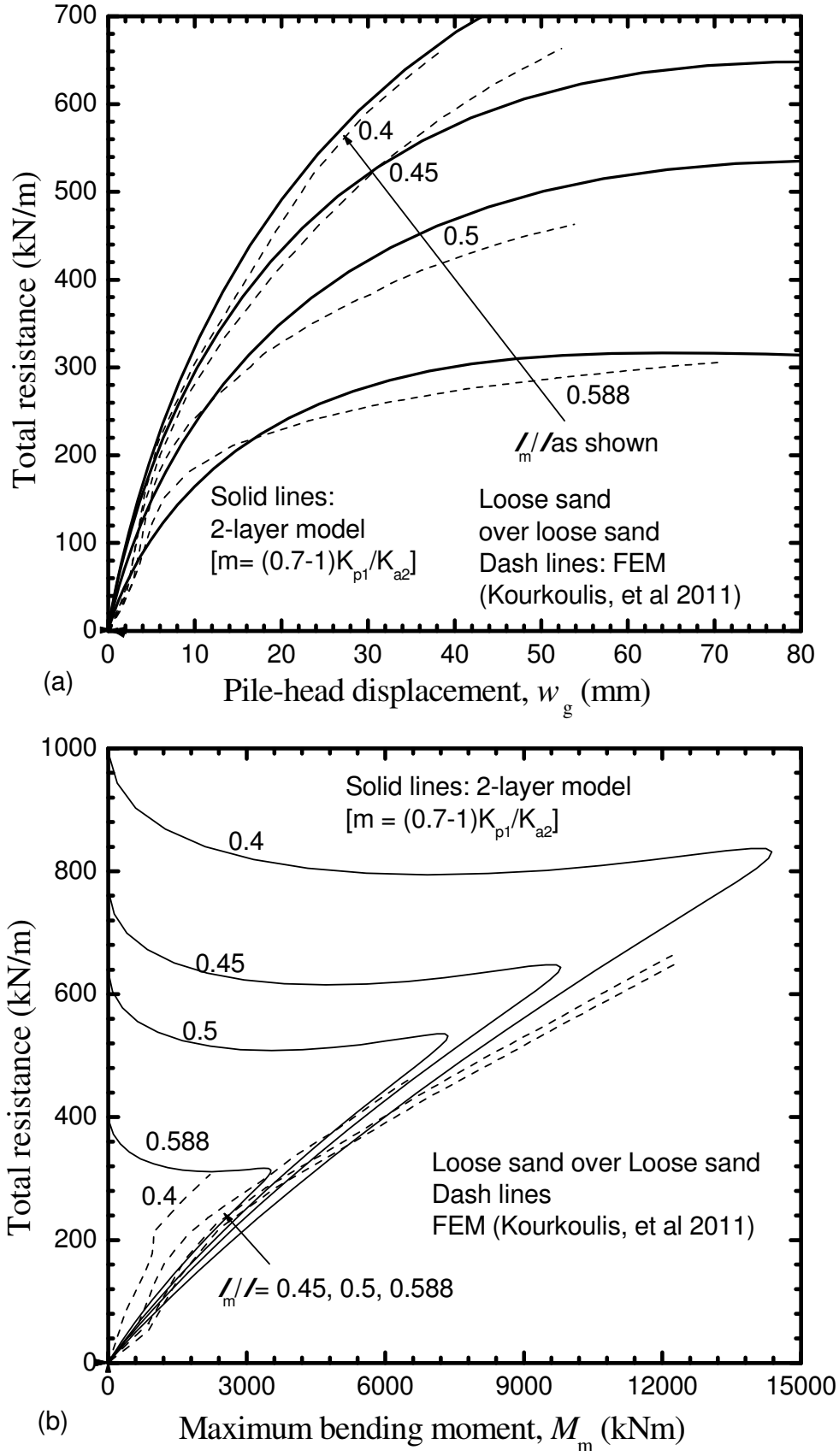

Figure 5 Predicted versus measured evolution of total thrust on piles in loose sand overlying loose sand: (a) pile-head displacement w_g, (b) maximum bending moment.

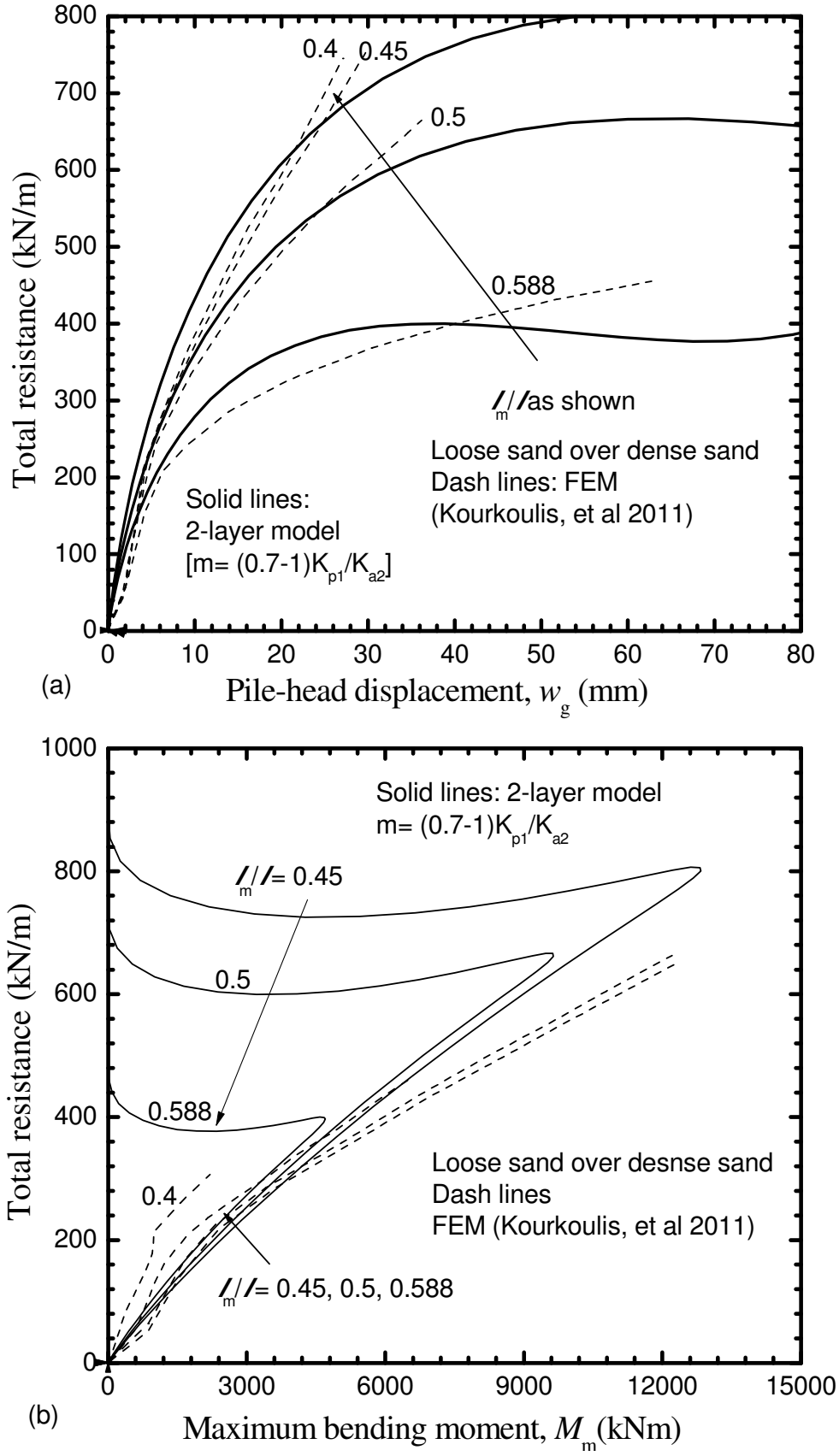

Figure 6 Predicted versus measured evolution of total thrust on piles in loose sand overlying dense sand: (a) pile-head displacement w_g, (b) maximum bending moment.

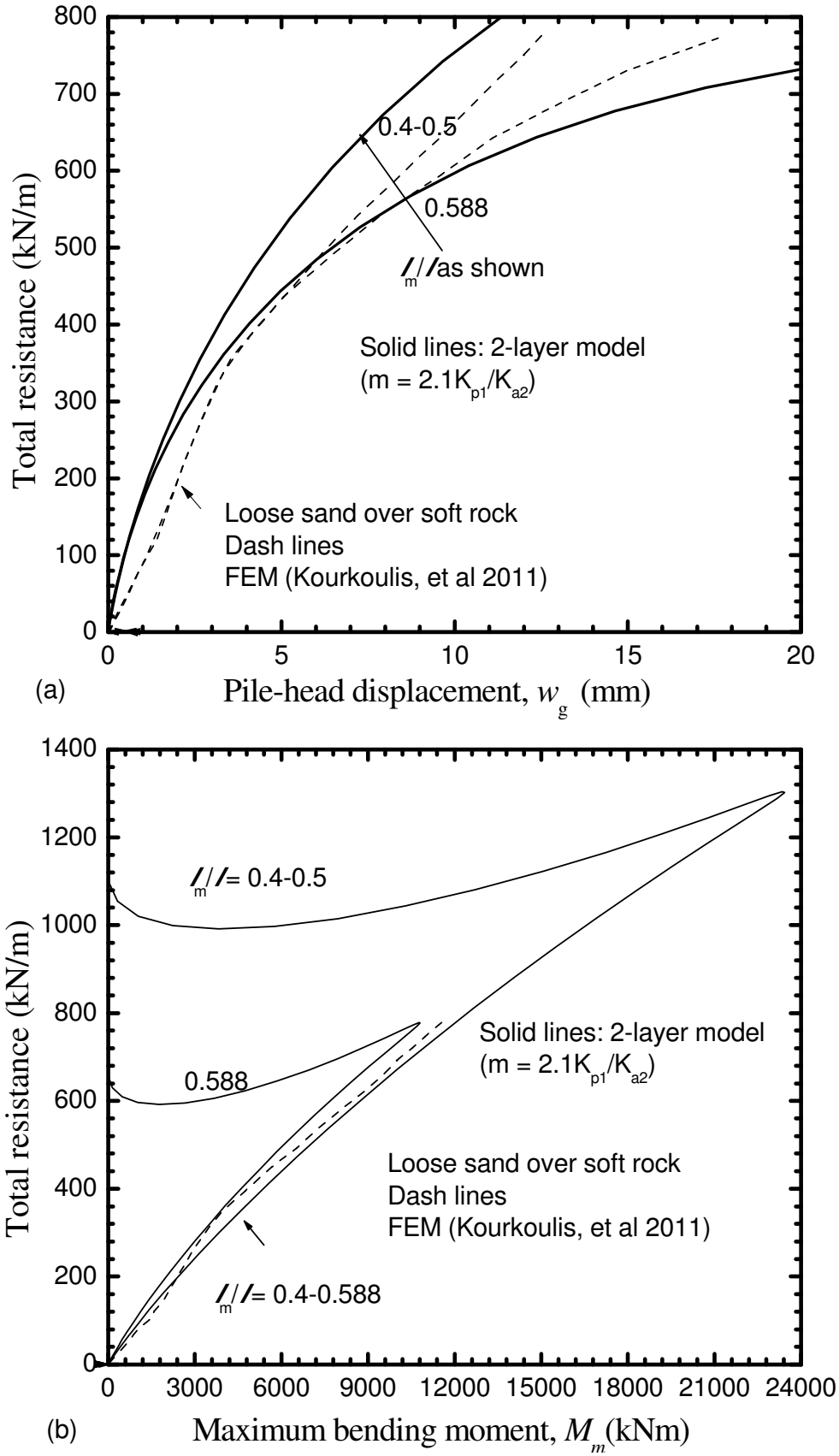

Figure 7 Predicted versus measured evolution of total thrust on piles in loose sand overlying soft rock: (a) pile-head displacement w_g, (b) maximum bending moment.

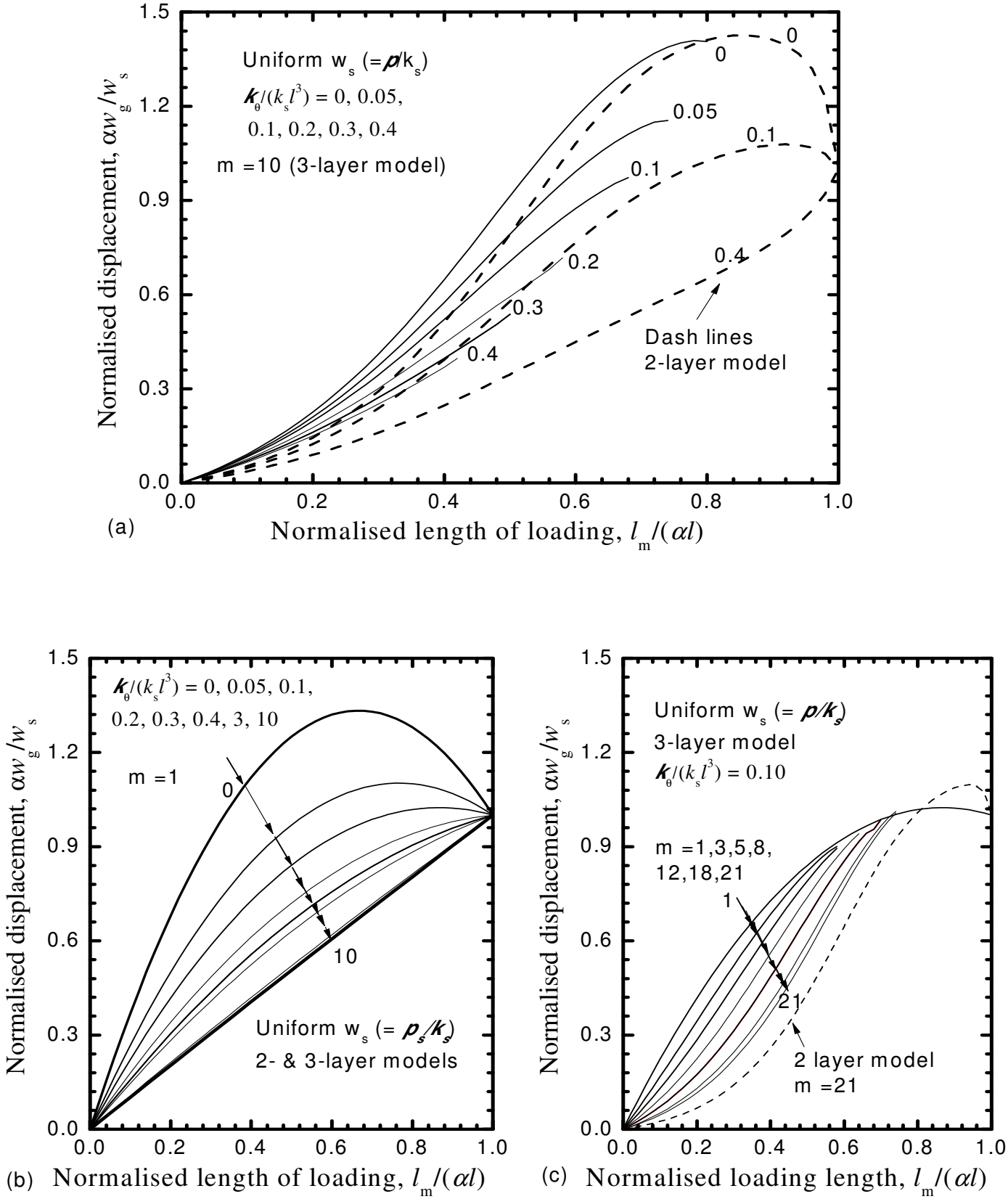

Figure 8 Normalized uniform soil movement w_g (constant k_s) with loading depth owing to (a) normalized rotational stiffness (m = 10), (b) normalized rotational stiffness (m = 1), (c) modulus ratio m ($\bar{k}_\theta$ = 0.1)

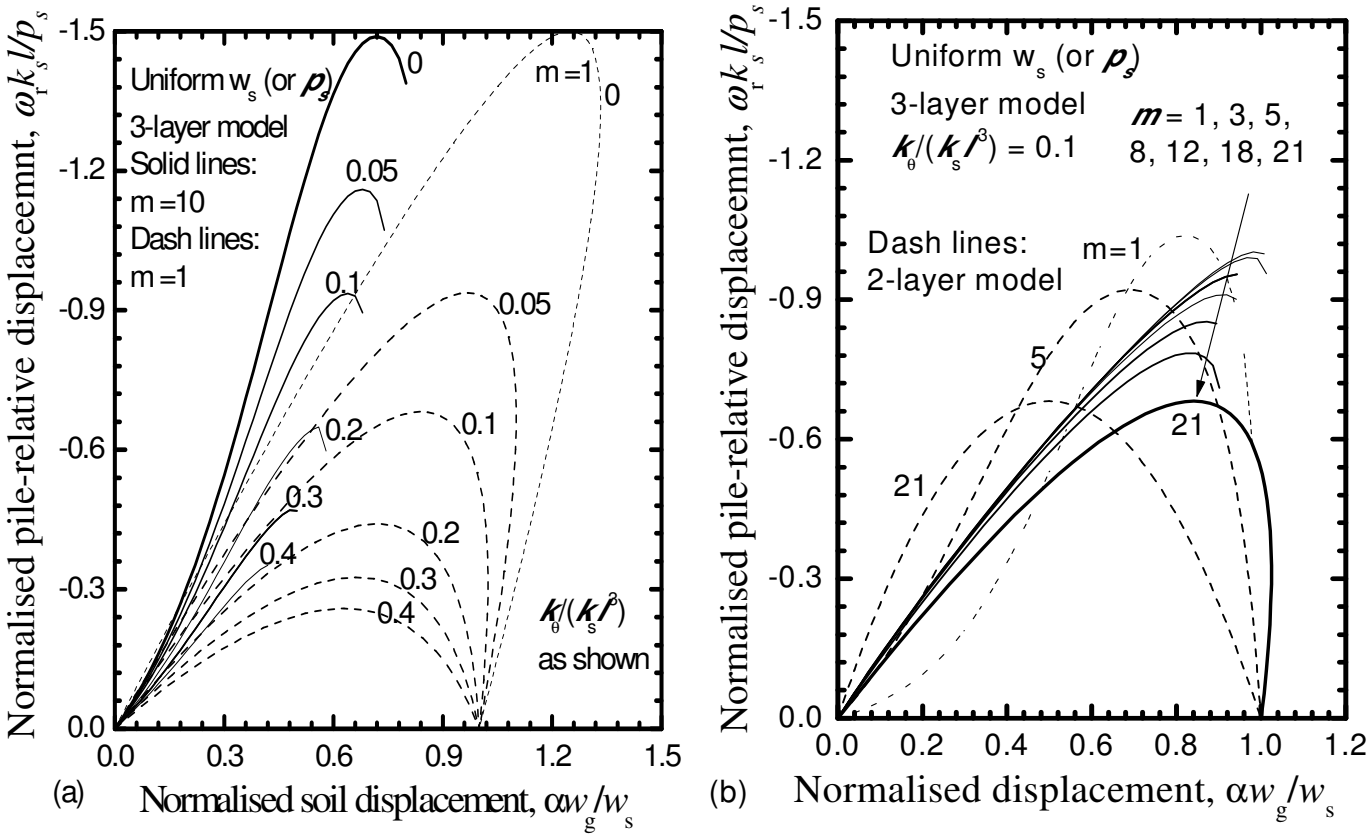

Figure 9 Normalized pile rotational displacement (constant k_s) versus normalized pile-head displacement owing to (a) normalized rotational stiffness (m = 10 or 1), (b) modulus ratio m ($\bar{k}_\theta$ = 0.1)

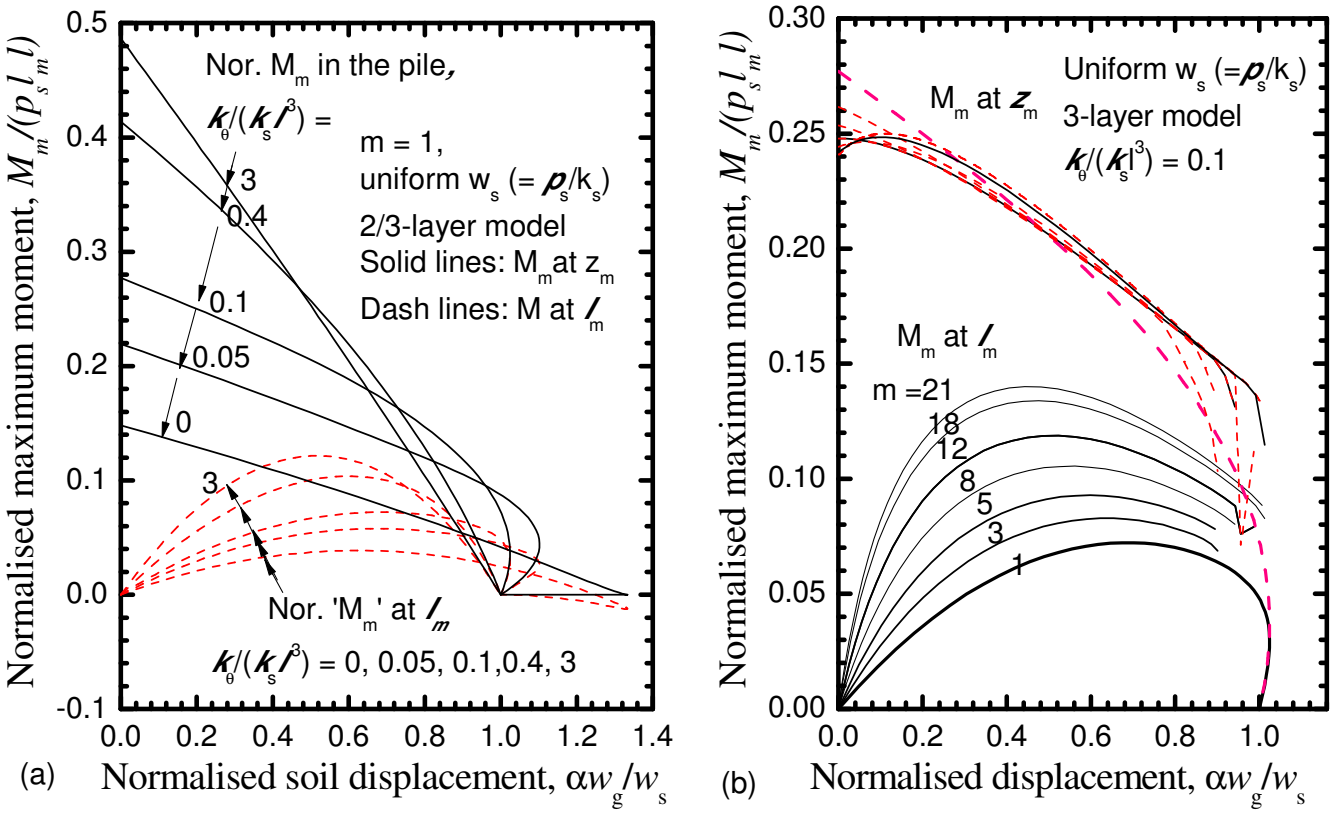

Figure 10 Normalized bending moment for base restrained piles with normalized soil movement w_s (constant k_s, and $k_B = k_\theta$) at z_m and l_m: (a) $\bar{k}_\theta$ = 0-3 and m = 1, (b) $\bar{k}_\theta$ = 0.1 and m =1-21

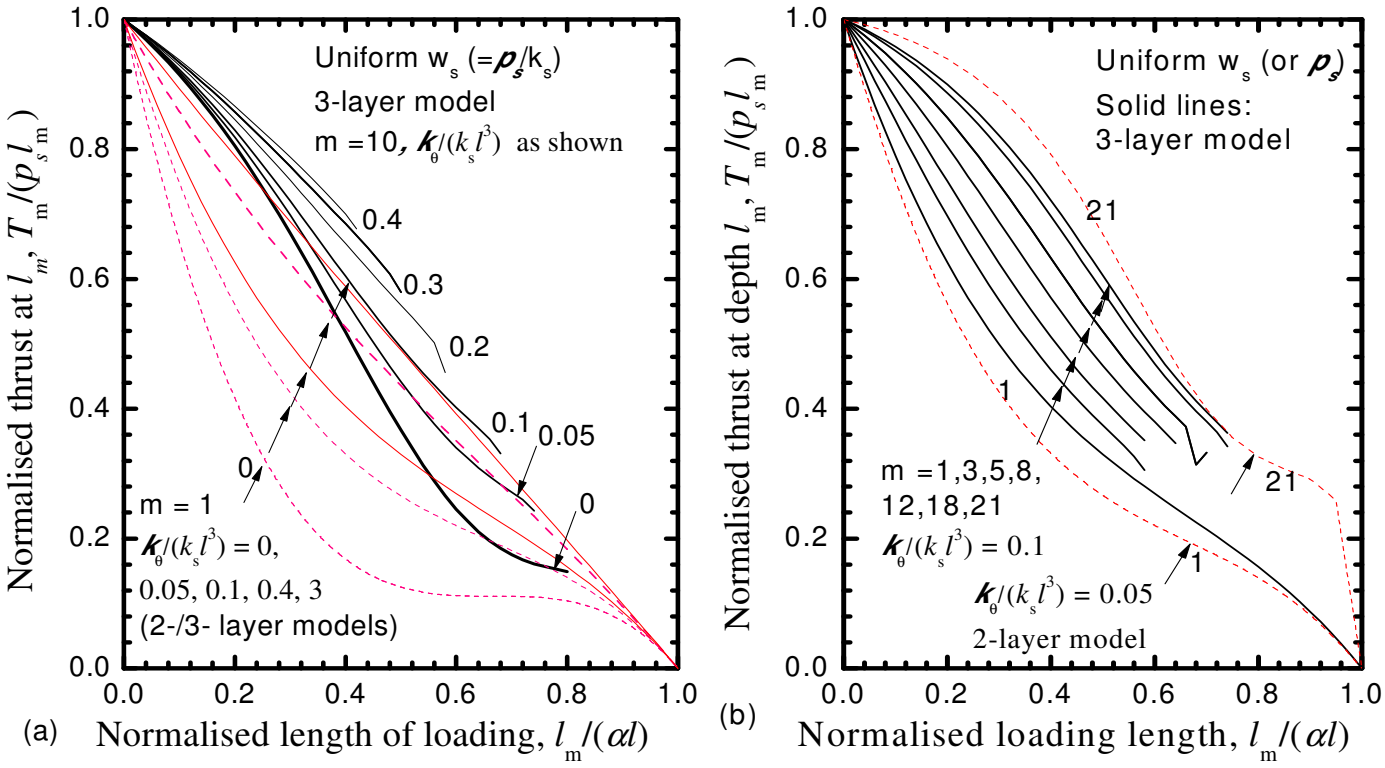

Figure 11 Normalized thrust at sliding depth owing to (a) normalized rotational stiffness (m = 10), (b) the modulus ratio m ($\bar{k}_\theta$ = 0.1/0.05)

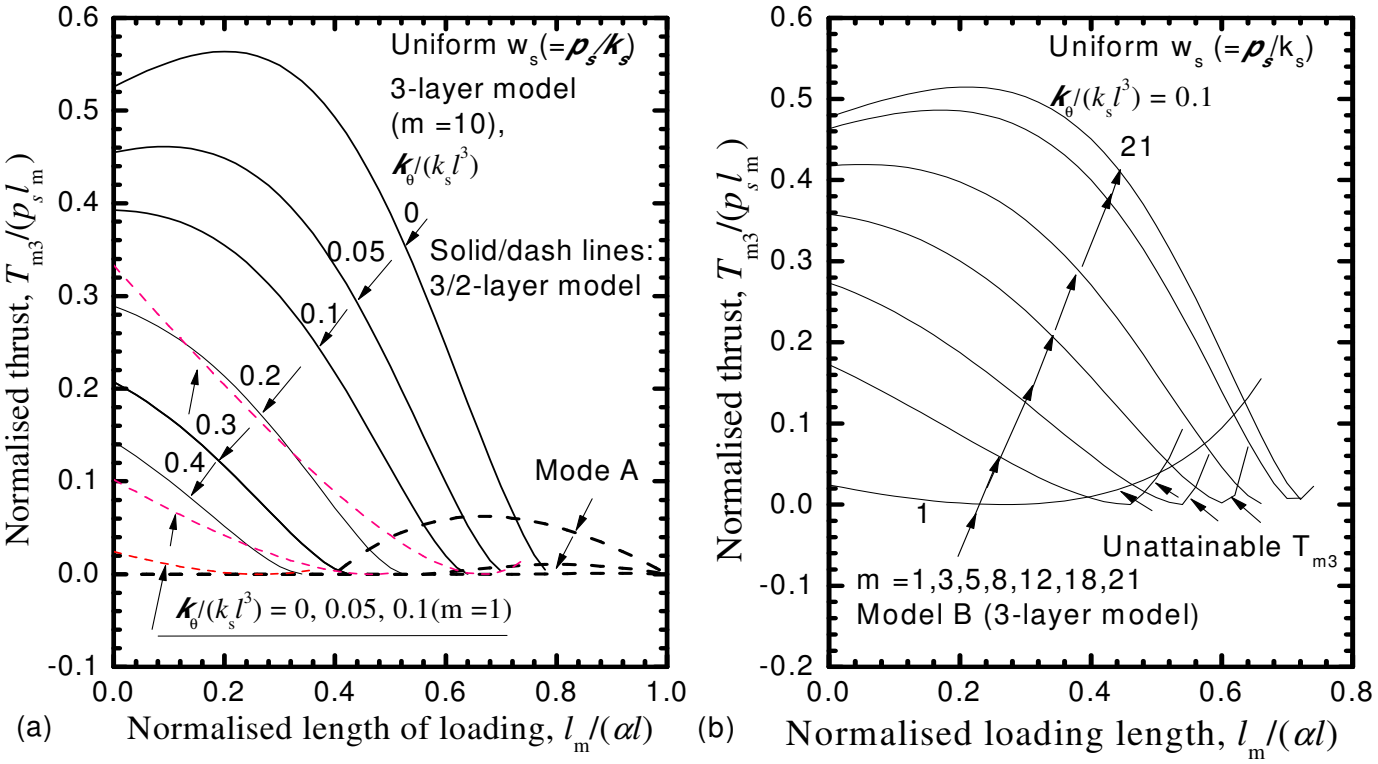

Figure 12 Normalized thrust T_{m} owing to (a) normalized rotational stiffness (m = 10), (b) the modulus ratio m ($\bar{k}_{\theta}$ = 0.1).

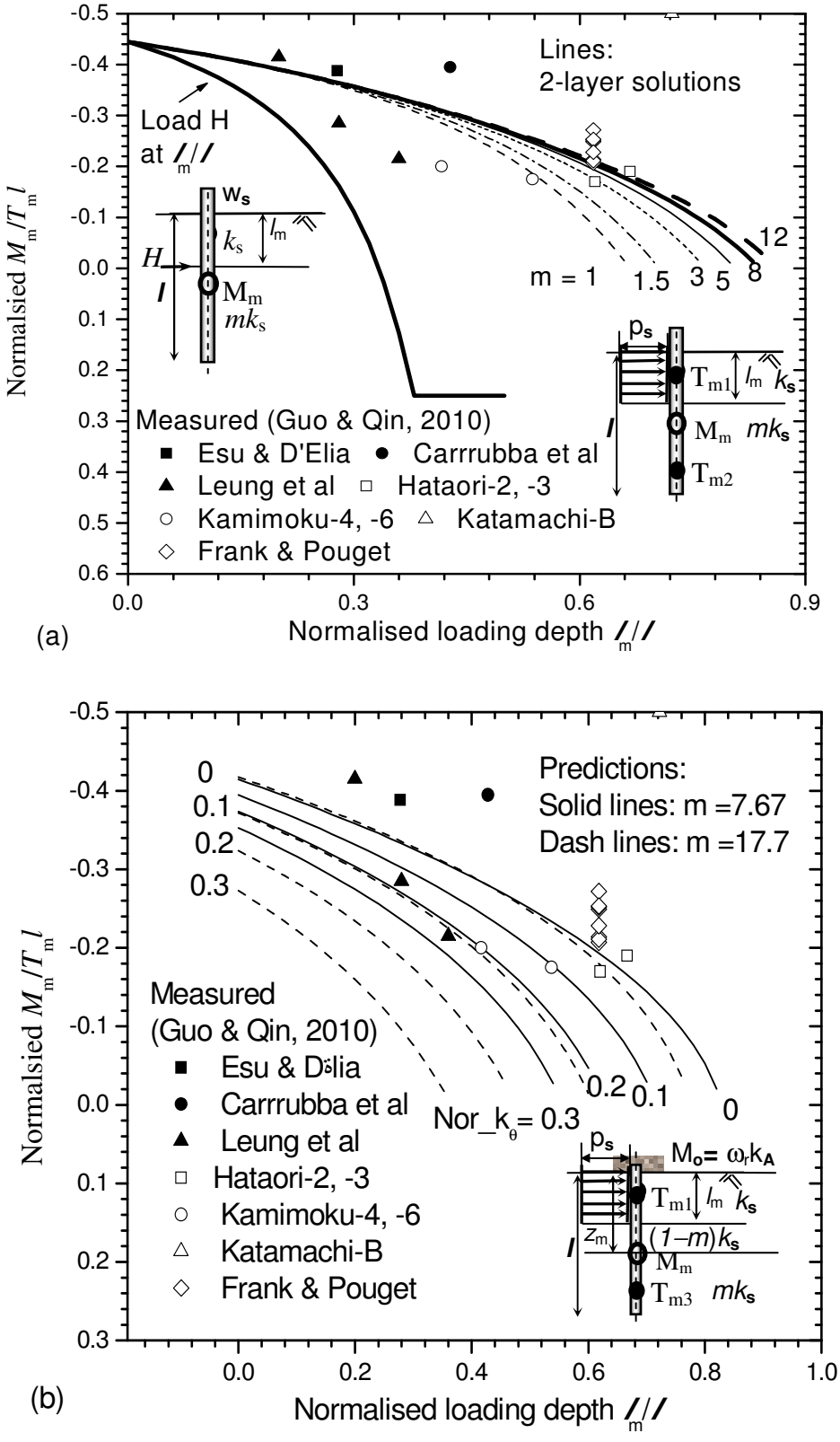

Figure 13 Predicted versus measured ratios of $M_m/T_m l$: (a) H-based and 2-layer model, (b) 3-layer model

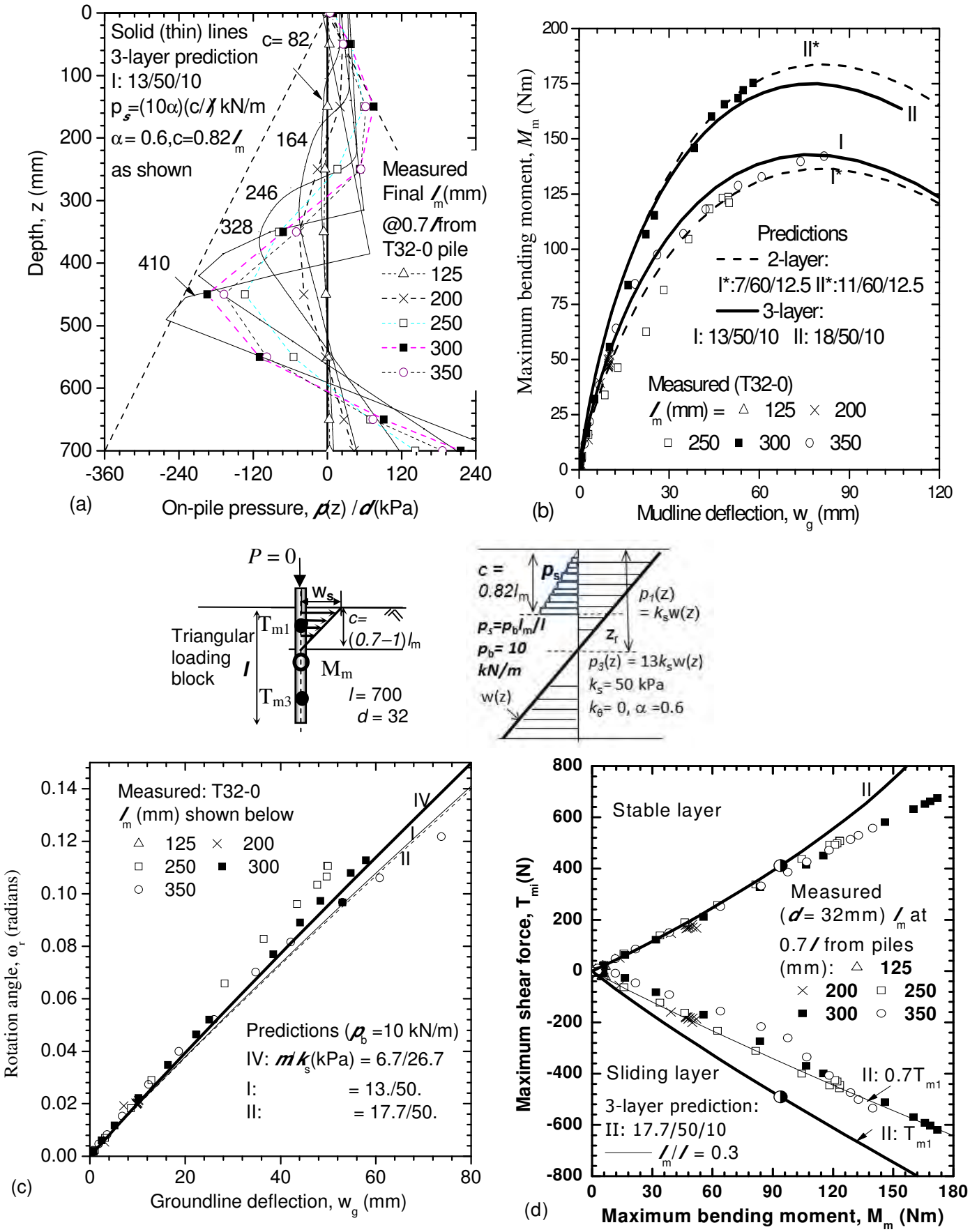

Figure 14 Predicted versus measured (a) on-pile pressure [9], (b) M_m ~ mudline displacement w_g curves, (c), (d) response of u_g ~ ω and M_m ~ T_{mi}, respectively [38]

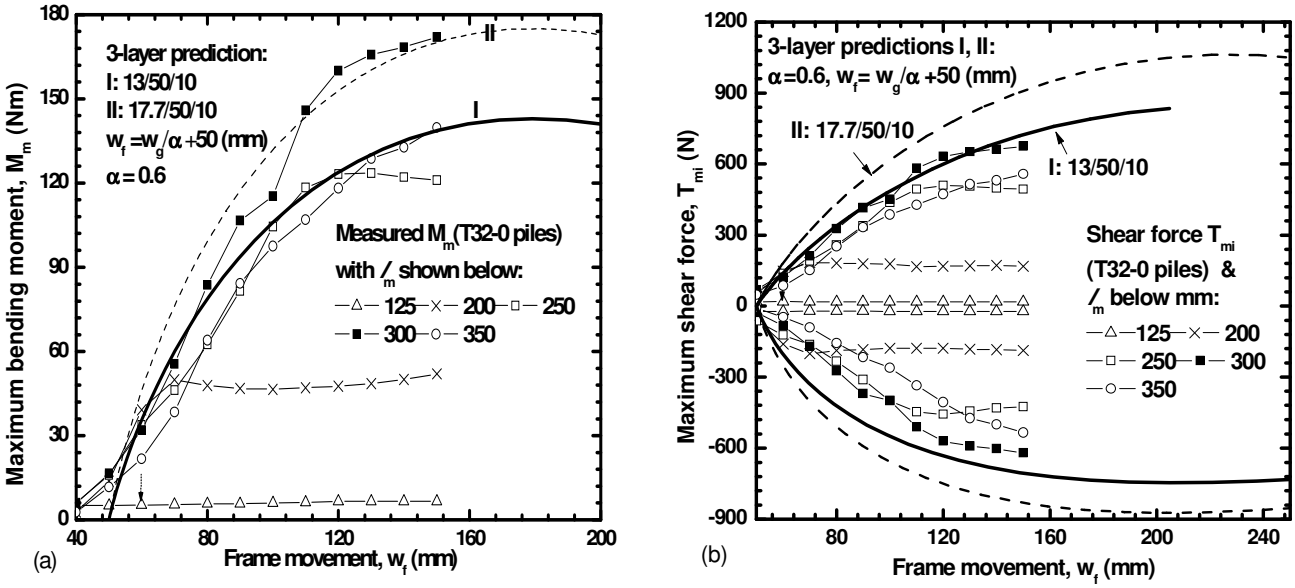

Figure 15 Predicted versus measured (a) bending moment M_m and (b) shear force T_{mi} with soil movement w_f

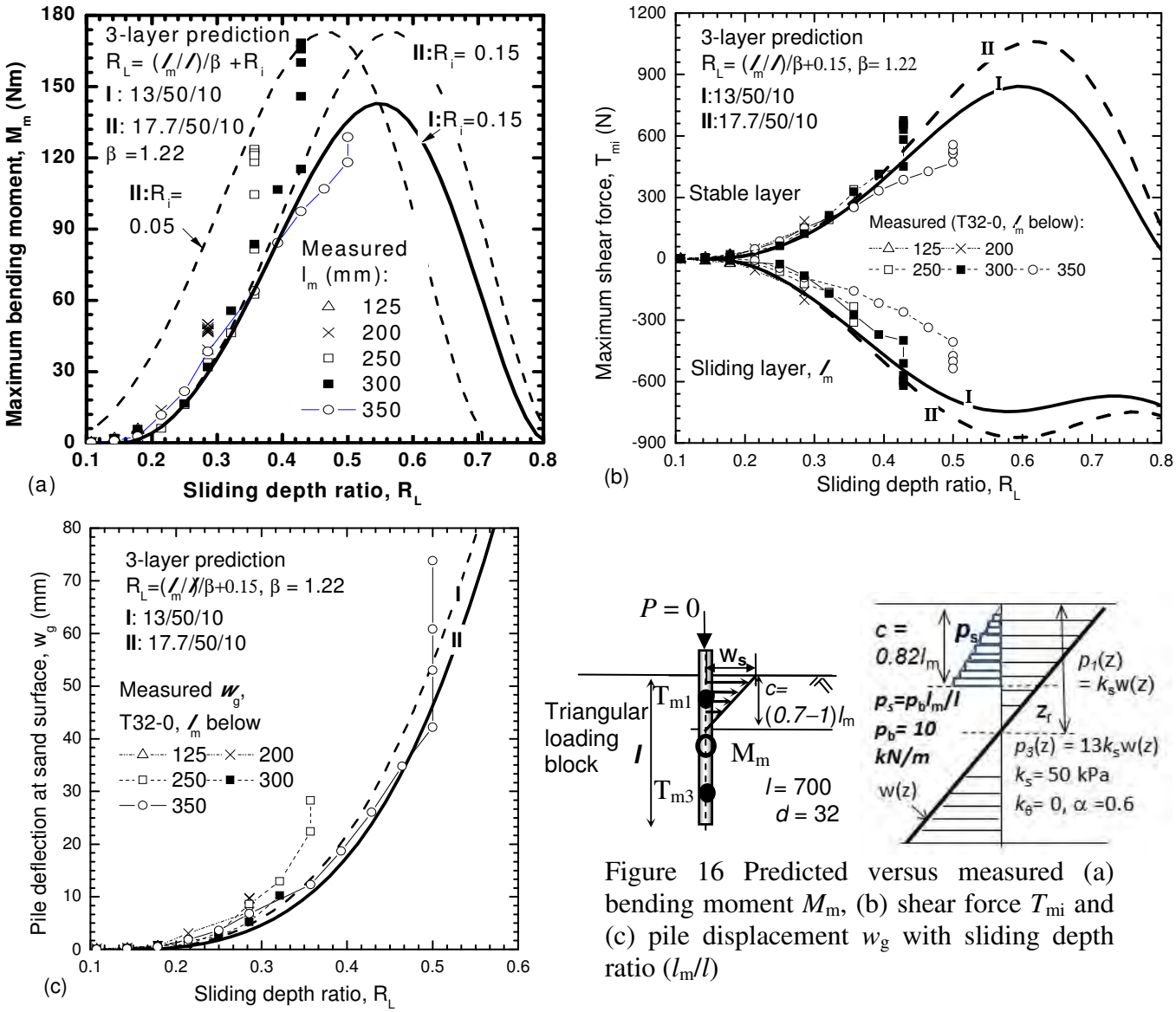

Figure 16 Predicted versus measured (a) bending moment M_m, (b) shear force T_{mi} and (c) pile displacement w_g with sliding depth ratio (l_m/l)

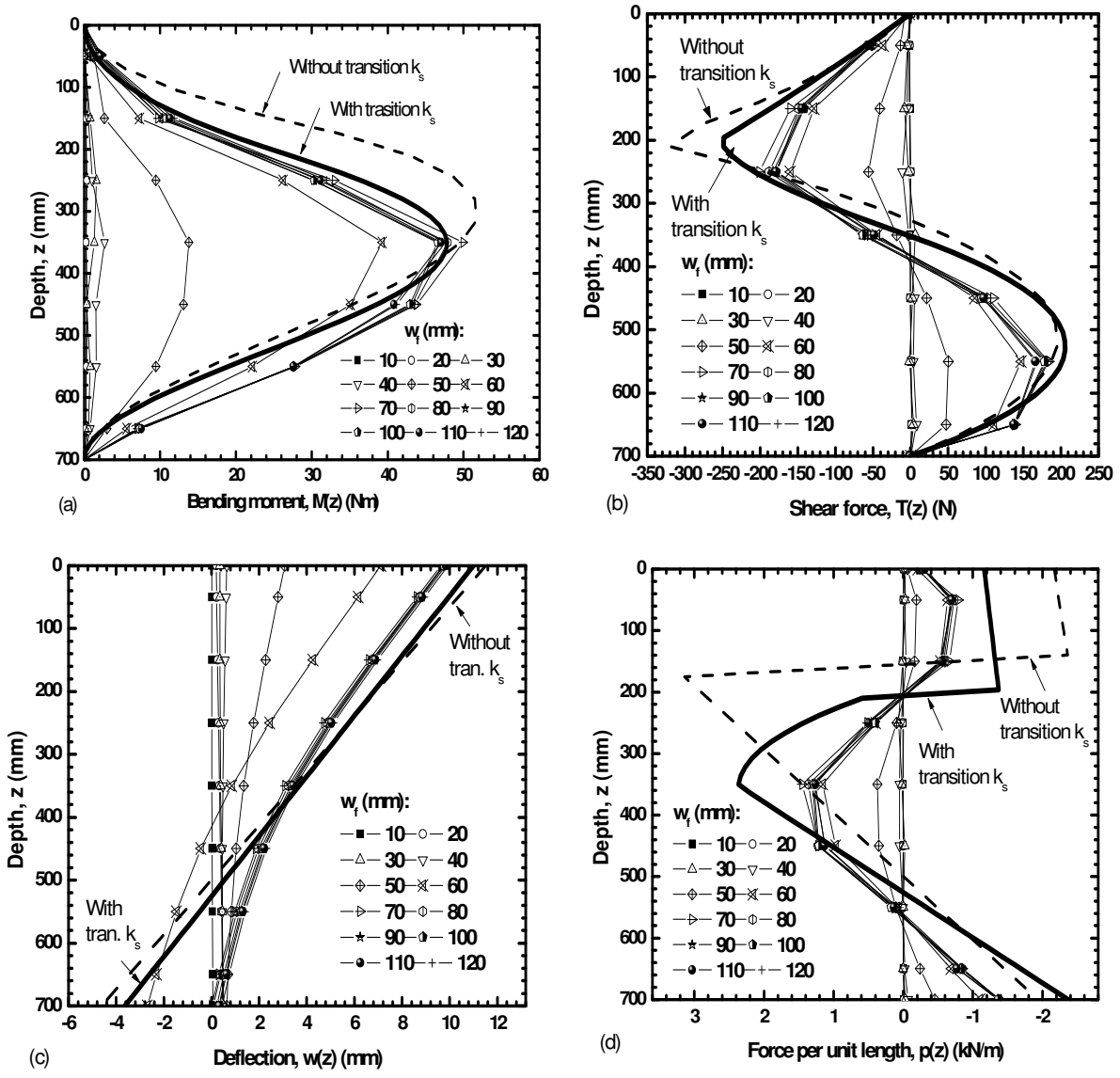

Figure 17 Responses of pile during TS32-0 using $m/k_s/p_b$ = 7/60kPa/12.5kN/m (2-layer model), or 13/50kPa/10kN/m (3-layer model prediction I): (a) Bending moment, (b) shear force, (c) pile displacement, and (d) on-pile force per unit length $p(z)$

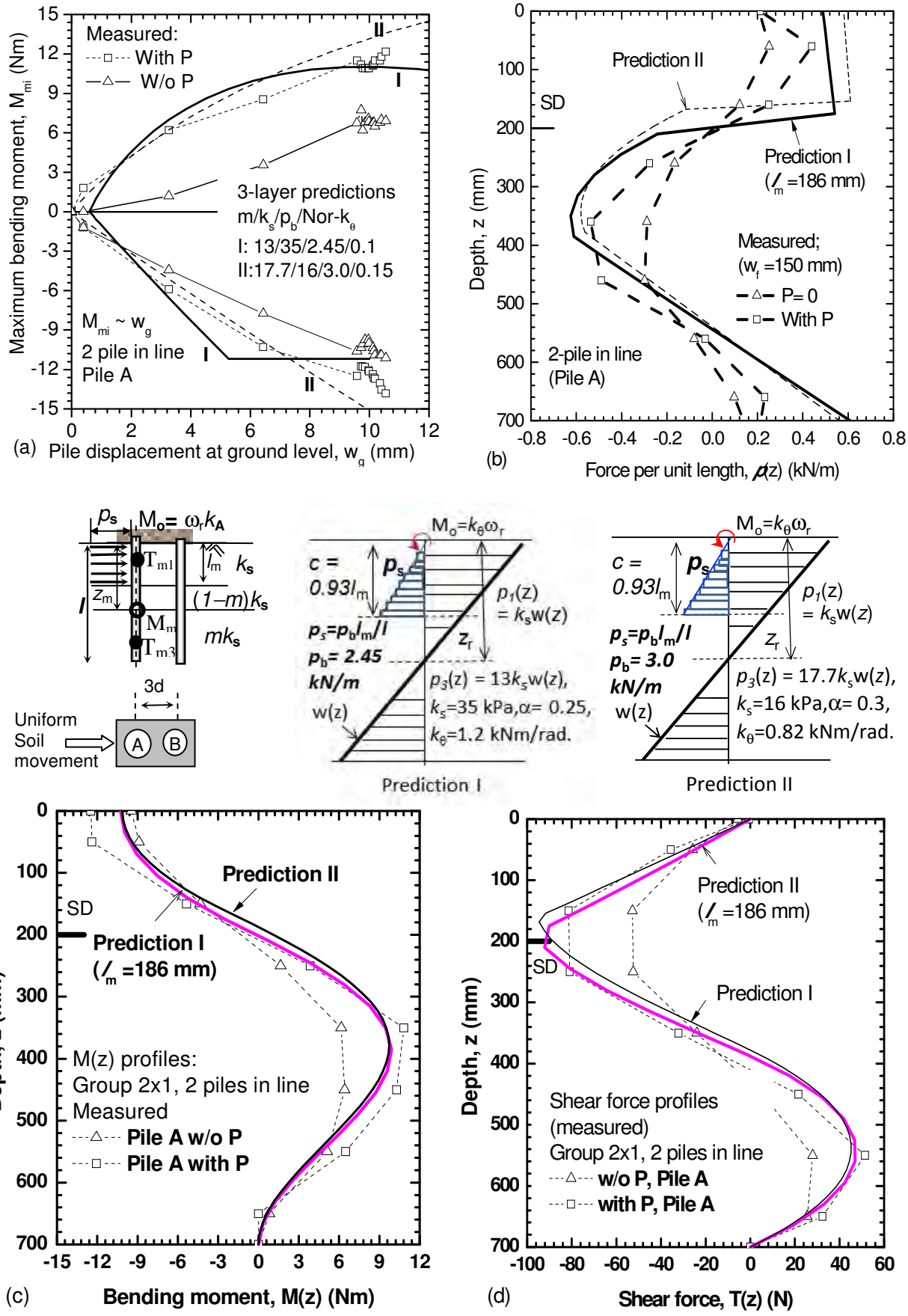

Figure 18 Predicted (3-layer model) versus measured [42] response of Pile A in 2-pile in-line group under a uniform soil movement: (a) Development of M_{mi} and w_{gi}, (b) on-pile force per unit length; (c) bending moment and (d) shear force profiles at ultimate state

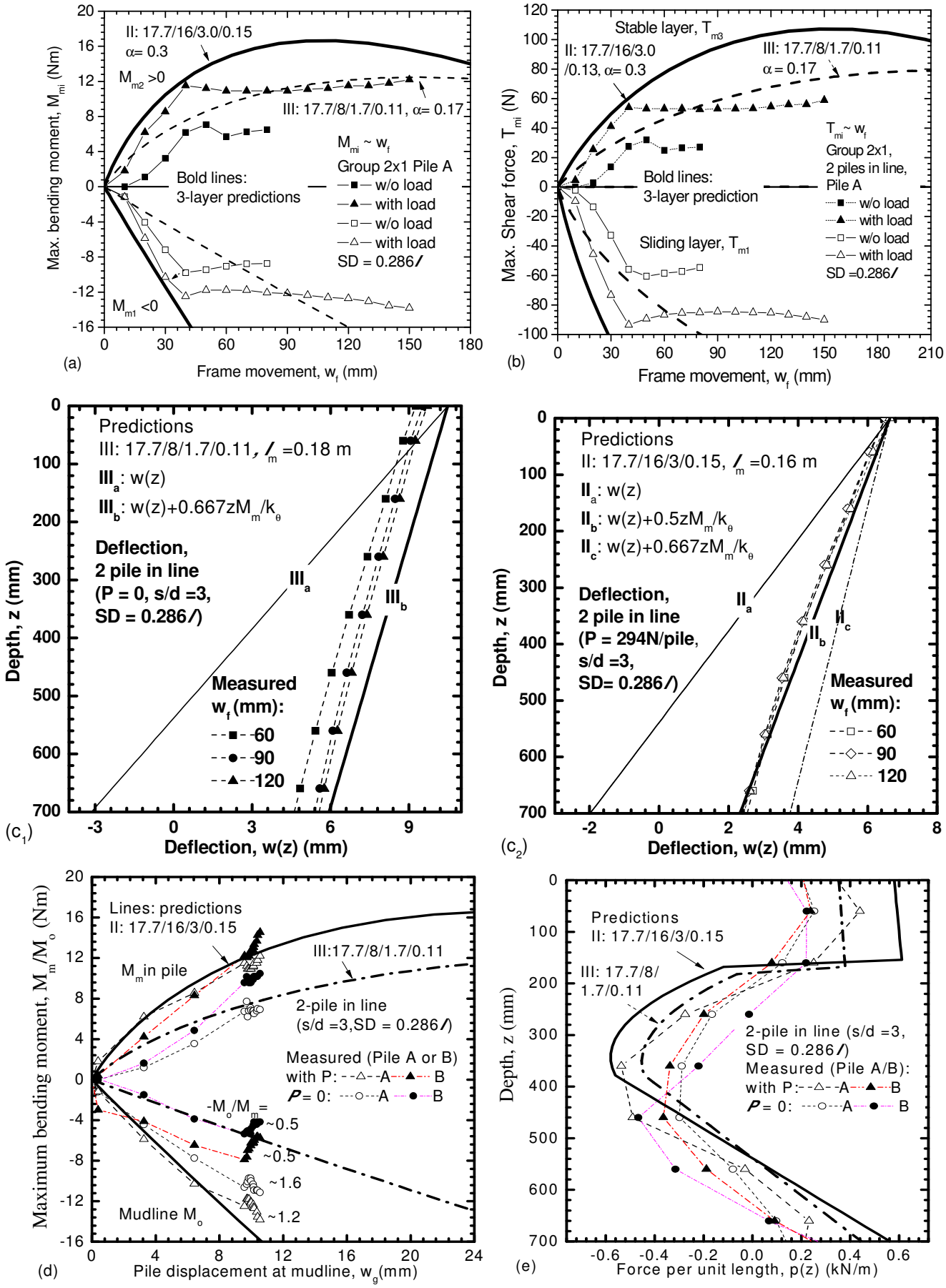

Figure 19 Predicted versus measured response of (a) $M_{mi} - w_f$, (b) $T_{mi} - w_f$, (c) $M_{mi} - w_g$, and (e_1, e_2) $w(z)$, (d) $M_{mi} - w_g$, and (e) $p(z)$ (2-pile in- line)

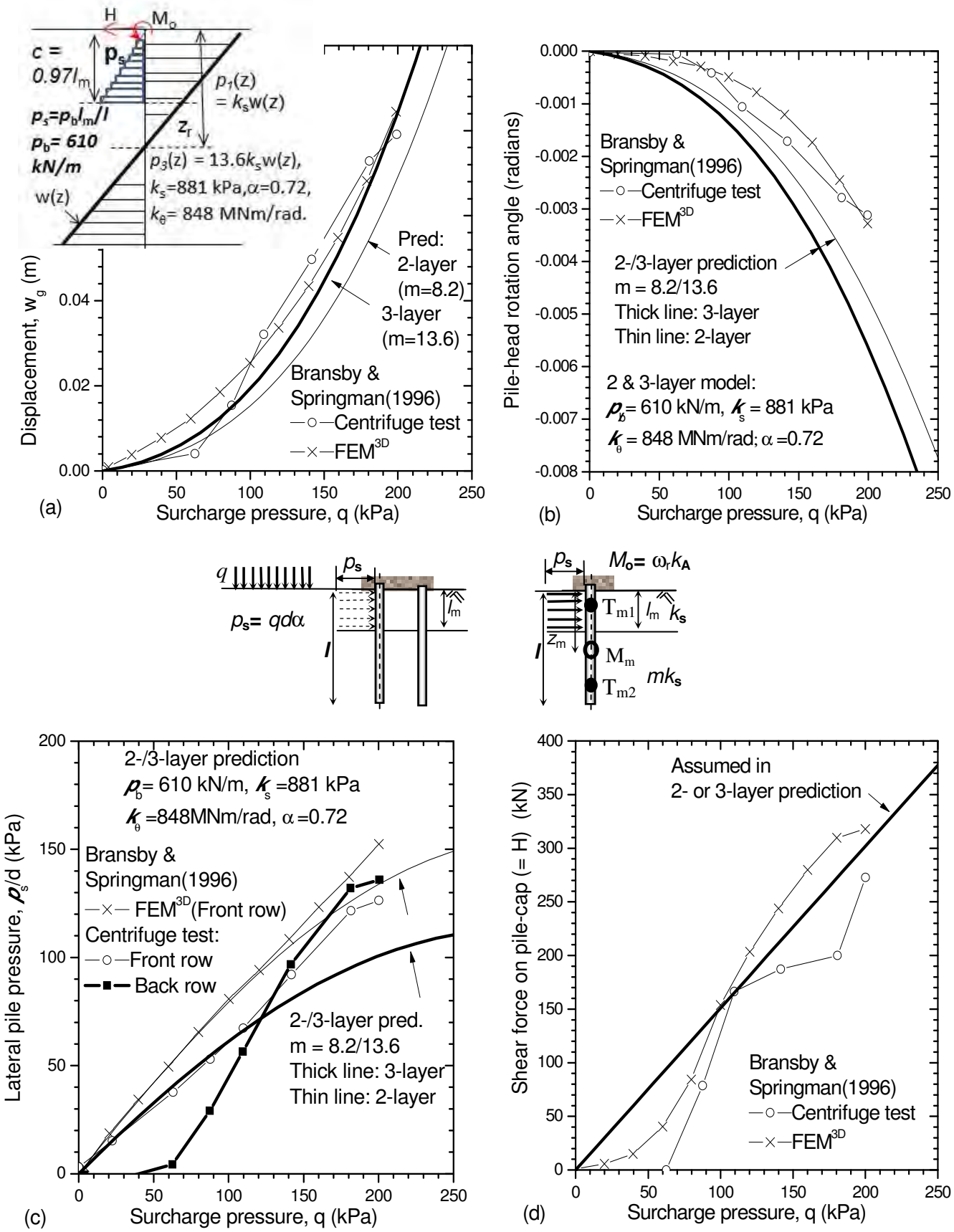

Figure 20 Predicted versus centrifuge test [14] of piles under typical surcharges: (a) pile-group displacement; (b) pile-rotation angle; (c) on-pile lateral pressure; and (d) shear force mobilised along the pile cap.

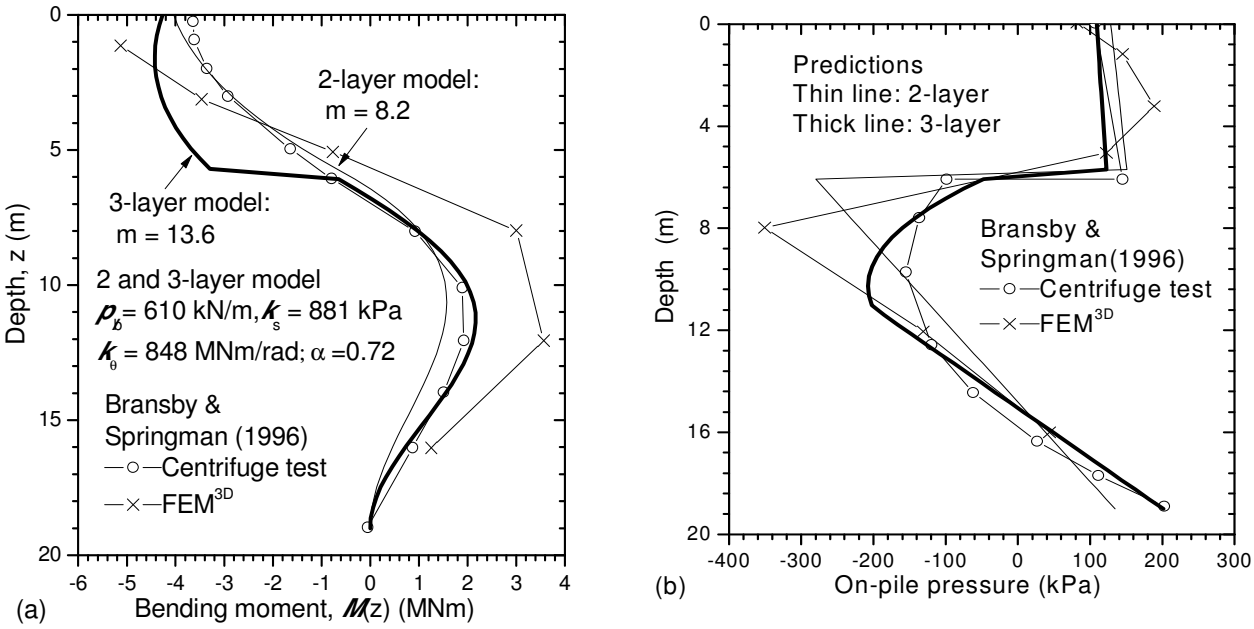

Figure 21 Predicted versus centrifuge test [14] under a surcharge of 200 kPa: (a) Bending moment profiles, (b) on-pile pressure profiles